

Nucleolar protein 7 facilitates melanoma progression and metastasis via HIF-1 α /PI3K/AKT/ERK axis

Yumei Li

Fuzhou University

Fan Chen

Fuzhou University

Weiyu Shen

Fuzhou University

Bifei Li

Fuzhou University

Ning Zheng

Fujian Medical University

Yusheng Lu

Minjiang University

Vladimir L. Katanaev

university of gevena

Lee Jia (✉ cmapcjia1234@163.com)

Fuzhou University

Research

Keywords: Nucleolar protein 7, cancer cell survival regulation, melanoma metastasis prevention, hypoxia/HIF-1 α signal, PI3K/AKT/ERK pathway

Posted Date: October 7th, 2020

DOI: <https://doi.org/10.21203/rs.3.rs-86056/v1>

License: © ⓘ This work is licensed under a Creative Commons Attribution 4.0 International License.

[Read Full License](#)

Abstract

Background

Metastasis is the cause of most fatalities in cancer patients and is poorly understood. Discovery of the underlying determinant and regulatory networks implicated in the cancer cell metastasis is urgently needed.

Methods

The expression pattern of nucleolar protein 7 (NOL7) was examined by IHC in clinic melanoma samples. Loss-of-function in melanoma cells was achieved through siRNA and CRISPR/Cas9 system. Assays for proliferation, apoptosis and aggressiveness were performed for functional verification. Immunoblotting and qRT-PCR were used to measure the alterations in proteins and mRNA. Orthotopic xenograft nude mouse model was established to assess the effects of NOL7 on melanoma tumorigenicity and metastatic potential.

Results

NOL7 expression was increased with melanoma progression. Abrogation of NOL7 expression led to the dysfunction of malignant behaviors including proliferation, invasion, and anoikis-resistance of melanoma cells *in vitro*. Depletion of NOL7 expression suppressed melanoma growth and metastasis *in vivo*. Mechanistically, NOL7 was found to be induced by HIF-1 α under hypoxic condition and inhibition of NOL7 reduced the phosphorylation of AKT and ERK protein.

Conclusion

This study revealed the cancer-promoting activity of NOL7 in melanoma cells and identified a novel regulatory mechanism of HIF-1 α /NOL7/PI3K/AKT/ERK axis in melanoma. NOL7 can function as a novel alert marker and therapeutic target for melanoma treatment.

Background

Although melanoma has become one of the most common cancers, it remains poorly understood, especially in terms of how gene regulatory networks affect its metastasis[1, 2]. As the most fatal and irretrievable component of melanoma development, the metastasis cascade consists of multiple sequential steps: invasion across ECM and entering the circulatory system; surviving in the circulatory system and avoidance of the anoikis resistance; anchoring to distant organs; and finally the formation of full-fledged lesions[3]. A fairly large number of early disseminated malignant cells detach from the primary tumor (> 1 million cells per gram of tumor per day)[4]. However, due to hostile tumor microenvironment factors, such as anoikis, immune cell pursuit and hemodynamic shear force, most of the detached cells become nonvital in the circulatory system. Only less than 0.1% of cancer cells can survive to drive the consequent metastasis cascade[5]. Cells' survival and metastasis are actuated by the

accumulation of inherent genetic and epigenetic evolutionary traits. Although the knowledge of genetic alterations and molecular mechanisms in melanoma development has advanced significantly over the past few years, far less is known about the genes that regulate cell survival and metastasis, and exhaustive knowledge of its regulation is lacking[6].

Nucleolar protein 7 (NOL7) functions as an RNA-binding protein that controls the fate of RNA from synthesis to degradation[7]. NOL7 is located in the nucleus including the nucleolus, and is encoded by NOL7 gene, which maps to the chromosome band 6p23[8]. NOL7 is poorly characterized and the role of NOL7 in cancer progression has been controversial in past reports. Some publications declared that NOL7 functioned as a tumor suppressor in cervical cancer through reversing the angiogenic phenotype[9, 10]. On the contrary, certain evidence also indicated that c-myc induced NOL7 expression to confer its oncogenic ability. In addition, researchers observed that inhibiting NOL7 expression in osteosarcoma cells inhibited cell proliferation *in vitro*[11, 12].

However, the role of NOL7 in the pathogenesis of melanoma has not so far been investigated. Herein, we aimed to obtain a deeper insight into NOL7 and discern its pivotal roles in melanoma, identifying this protein as a tailored marker of advanced and metastatic melanoma and as a therapeutic target to fight melanoma progression and metastasis.

Methods

Cell, cell culture and establishment of pulmonary metastasis cell lines

The mouse melanoma cell line B16F10 and the human melanoma cell line A375 were procured from Cell Resource Center of the Shanghai Institute for Biological Sciences (Chinese Academy of Sciences, Shanghai, China). Established post-metastasized melanoma cells, B16F10M and A375M were derived from the pulmonary metastases formed in mice by tail vein injection of pro-metastasized parental B16F10 and A375 cells, respectively, via a primary cell line establishment method[13,14]. This experimental metastasis refers to the injection of tumor cells directly to the systemic circulation and circumvents the invasion and extravasion.

The cells mentioned above were cultured in RPMI 1640 medium (Hyclone, Logan, UT, USA). Human pulmonary microvascularendothelial cells (HPMECs) were purchased from Cell Resource Center of the Shanghai Institute for Biological Sciences and cultured in ECM medium (Hyclone). All culture media was supplemented with 10 % (v/v) fetal bovine serum (FBS, Gemini Bioproducts, West Sacramento, CA) and 100 µg/mL penicillin/streptomycin (Sigma-Aldrich, St Louis, USA). Cells were maintained in a humidified atmosphere with 5 % CO₂ at 37°C. Low oxygen concentration (1 % O₂) was controlled by 245 whitley H35 HEPA hypoxystation (UK) or treated with YC-1 (MedChem Express, Princeton, NJ, USA). The cell lines were authenticated by Genetic Testing Biotechnology Corporation (Suzhou, China) using short tandem repeat (STR) markers. Cells were collected with 0.25 % trypsin (Hyclone) and counted by the ADAM MC Auto Cell Counter (NanoEnTek, Korea) before used.

Antibodies and reagents

The following antibodies were used: anti-NOL7 (#DF9720), anti-p-Smad2/3 (AF3367) from Affinity Biosciences (Cincinnati, OH, USA); anti-PCNA (#PC10), anti-E-cadherin (#3195), anti-N-cadherin (#13116), anti-Vimentin (#5741), anti- β -catenin (#8480), anti-p21 (#2947), anti-p27 (#3686), anti-CDK2 (#2546), and anti-MMP9 (#13667), anti-Smad2/3 (D7G7) from Cell Signaling Technologies (Beverly, MA, USA); anti-AKT 1/2/3 (#sc8312), anti-p-AKT 1/2/3 (Ser 473, #sc33437), anti-ERK 1/2 (#sc135900), anti-p-ERK 1/2 (Thr 202/Tyr 204, #sc16982) and anti-Twist (#sc81417) from Santa Cruz Biotechnology, Inc. (Santa Cruz, CA); anti-JNK (#WL01295), anti-p-JNK (#WL01295), anti-HIF-1 α (#WL01607), anti-Gsk3 β (#WL0146), anti-caspase 3 (#WL02117), anti-caspase 9 (#WL01551), anti-bad (#WL02304), anti-bax (#WL01637), anti-survivin (#WL03492), anti-cyclin A (#WL01841) and anti-cyclin E (#WL01072) from Wanlei Biotechnology (Shenyang, China); anti-Fibronectin (#40932) from SAB Technology (Danvers, USA); anti-TSP-1(A2125), anti-Rb (A3618) from ABclonal Technology (Wuhan, China); β -actin (AC001-R), secondary antibody goat anti-mouse-IgG horseradish peroxidase and goat anti-rabbit-IgG horseradish peroxidase from Dingguochangsheng Biotechnology (Beijing, China).

NOL7 siRNA (sense, 5'-3', GCUGUAUUAGAGCAGCUAATT) for B16F10 cells, NOL7 siRNA (sense, 5'-3', GGAAAUGACUCCAAGAAAGATT) for A375 cells, corresponding negative control siRNA (UUCUCCGAACGUGUCACGUTT) and NOL7 guide RNA sequences (sgRNA, sense, 5'-3', CACCGACCGGAGCGTCTCGCGCCC) for A375 cells were synthesized by Sangon Biotech (Shanghai, China).

Gene constructs and generation of stable transfectants

Specific siRNAs were used for the transient knockdown of NOL7 in B16F10 and A375 cells. CRISPR/Cas9 system was operated to generate the stable NOL7-knockout A375 cells based on a previous protocol[15]. In short, sgRNA for A375 cells was designed by a CRISPR design platform (Zhang Feng Lab, <http://crispr.mit.edu/>) and then cloned into the PX458 vector. The empty vector was used as a control. These oligo duplexes were transfected into cells via Lipofectamine 3000 Kit (Invitrogen, MA, USA) through standard procedure. Furthermore, stable NOL7-knockout cells were sorted through GFP-activated cell sorting method by flow cytometer (FACS Aria III, BD, San Diego, USA).

Cell proliferation assay

For cell growth kinetic assay, NOL7-knockdown melanoma cells or control cells were plated in 96-well plates (5×10^3 cells/well). Cell proliferation was monitored every day for 5 days using cell counting kit-8 assay (Promega, Sunnyvale, CA) according to the manufacturer's protocol.

For cell spherical growth assay, A375-sgNOL7 cells or control cells were put into 96-well microplates with ultralow attachment surfaces (Corning). Visually 3D cell spheroids were formed after 24 h, and their growth was observed and photographed at regular time intervals by phase contrast microscopy to monitor the tumor spheres diameter.

Colony formation assay

A total of 1000 target cells per well were plated in 6-well plates. After culture in complete medium for 14 days, cell colonies were washed three times with PBS and fixed in 4 % paraformaldehyde for 20 min and then, stained with a 0.2 % crystal violet (Sigma-Aldrich) solution for 40 min at room temperature. An overall image of the cell colonies was mapped by Canon scanner (Shanghai, China). Colonies with 50 or more number of cells were counted under a light microscope (Zeiss, Oberkochen, Germany).

Cell cycle assay

Suspended cells were washed twice with precooled PBS and fixed in 70 % ethanol for 24 h at 4°C. The cells were then stained with a fluorescent solution (1 % (v/v) Triton X-100, 0.01 % RNase, 0.05 % PI (Sigma-Aldrich)) for 30 min at 37°C in the dark. Ten thousand events were acquired by flow cytometry to measure the cell cycle distribution. Data were processed by Modfit software 3.2.

Cell apoptosis assay

Using an Annexin V-FITC/PI kit (KeyGen Biotech, China), cell apoptosis was detected by flow cytometry. Target cells at a density of 3×10^5 cells per well were plated in 6-well plates in triplicate. The cells were preprocessed under the following conditions: one group of cells was cultured in complete medium; one group of cells was treated with 10 μ M paclitaxel (Meilunbio, Dalian, China) and another group of cells was kept in a suspended state or in FBS-free medium. All of these cells were collected separately after 24 h, and stained with Annexin V-FITC/PI for 15 min under the lucifuge condition. At least 10^4 cells from each specimen were examined by flow cytometry and data were analyzed by FlowJo software 10.0.

Domestication of anoikis-resistant A375 cells

Anoikis-resistant A375 cells were generated through continuous cycle of culturing on normal (adherent) and soft agar (Sigma-Aldrich) -coated cell culture well (suspended). Briefly, A375 cells were plated in soft agar-coated wells and maintained under suspended conditions for the indicated time intervals. After 24 h incubation, cells were washed and transferred to normal cell culture wells. We measured the anoikis-resistance of A375 cells by analyzing the cells apoptosis.

In vitro cytotoxicity assay

A MTT (3-(4,5-dimethylthiazol-2-yl)-2, 5-diphenyltetrazolium bromide, Sigma-Aldrich) assay was used to assess cell sensitivity to paclitaxel, an broad spectrum anticancer drug[16]. The cells were plated in 96-well plates at a concentration of 10^4 cells/0.1 mL per well. The cells were treated with various concentrations (0-100 μ M) of paclitaxel for 24 h. Finally, the culture medium was replaced with MTT solution (5 mg/mL in phenol red or serum-free medium) and incubated for an additional 4 h. Formazan crystals formed by metabolically viable cells were dissolved in 150 μ L DMSO. Absorbance at 490 nm was recorded by an Infinite M200 Pro microplate reader (Tecan, Hombrechtikon, Switzerland).

Motility assay

Cell motility was measured by wound healing assay. Monolayer cells in 6-well plates were scratched with a 100 μ L pipette tip ($t = 0$ h) and maintained in 1640 medium containing 1 % FBS. The wounded area was photographed at 0 h and 24 h by a light microscope (Zeiss). Cell mobility was quantified as the difference value between the width of the wound at a given time and the initial width of the wound.

Migration and invasion assays

Falcon cell culture inserts with 8 μ m pores (Corning, Cambridge, MA, USA) were placed in 24-well plates. To measure invasion, the upper chamber of a Transwell apparatus was precoated with Matrigel (Corning). Cells in 200 μ L culture medium containing 1 % BSA were plated into the upper chamber and 800 μ L culture medium containing 20 % FBS was added to the lower chamber. After incubation for 24 h, the noninvasive cells that adhered to the upper chamber were wiped away, while the invasive cells adhered to the lower chamber were fixed with 4 % paraformaldehyde for 30 min and stained with crystal violet for 40 min. The invasive cells per field were assessed by a fluorescence microscope (Zeiss). To measure cell migration, the upper chamber of the inserts was not precoated with Matrigel.

Adhesion assay

To measure cells adhesion to endothelial cells, monolayer HPMECs were precultured in 6-well plates and stimulated with IL-1 β (10 ng/mL, Sigma-Aldrich) for 4 h. Subsequently, the target cells labeled with rhodamine 123 (Sigma-Aldrich) came into contact with the surface of HPMECs and oscillated at 200 rpm for 30 min. After that, the cells that didn't attach to the HPMECs were washed away gently. The cells adhered to HPMECs were photographed and counted by phase-contrast light microscopy (Zeiss). Similarly, to measure adhesion to the ECM, rhodamine 123-labeled target cells were plated into 6-well plates with fibronectin-coated (Sigma-Aldrich) and incubated without shaking for 30 min.

Western blotting

Cell lysates were extracted by RIPA lysis buffer containing 1 μ M PMSF at 4°C. Then each equal quality of each sample was separated by SDS-PAGE and transferred to PVDF (Bio-Rad, USA) membranes. After blocking in 5 % skim milk solution for 2 h at room temperature, the PVDF membranes were incubated with dilute primary antibodies overnight at 4°C and secondary antibodies at room temperature for 2 h. Protein blots were visualized using the hypersensitive chemiluminescence kit (Wanlei, Shenyang, China) through ChemiDoc XRS system (Bio-Rad). Protein expression levels were analyzed by Image Lab analysis software 5.0 (Bio-Rad). β -actin was served as the internal control.

Quantitative Real-Time PCR

Total RNA was extracted using TRIzol reagent (Invitrogen), and 100 ng of each sample was then used as template for reverse transcription to cDNA via a PrimeScript® reverse transcription kit (Takara, Japan) in accordance with the manufacturer's guide. PCR was performed by SYBR® Premix Ex Taq™ PCR kit (Takara) on a CFX96™ real-time PCR detection system (Bio-Rad). The threshold cycle values were used to

quantify the relative mRNA expression and normalized to β -actin. Primer sequences used are listed in Supplementary Table 1.

Mice and in vivo mouse study

The mice experiment was guided and approved by the Institutional Animal Care and Use Committee (IACUC) of Fuzhou University, the approval number is SYXK-2019-0007. Female BALB/c nude mice 6-8 weeks old and female C57BL/6 mice 6-8 weeks old were obtained from Slac Animal Inc (Shanghai, China). BALB/c nude mice were housed in clean and sterile cage (Sujingantai Biotechnology, Suzhou, China) and fed with sterilized rat food (Fuzhou Wushi Animal Center, Fuzhou, China). and sterilized water. C57BL/6 mice were housed in clean cage and fed with usual rat food (Fuzhou Wushi Animal Center) and clean water. All mice were accessed to food and water ad libitum. The animal house was kept in a 12 h-day/night cycle with lights on at 7:00 a.m and in a temperature ($26 \pm 1^\circ\text{C}$) and humidity ($50 \pm 10\%$). All mice were randomised into each group by picking random numbers. The mice in all experiments involved in this manuscript were not given any drugs or anesthetic. We have tired our best to minimize animals' pain and suffering.

To obtain the pulmonary metastases of melanoma described above, B16F10 cells (5×10^4 cells in 0.1 mL PBS per mouse, 5 mice per group) were injected into the tail vein of C57BL/6 mice and A375 cells (3×10^6 cells in 0.1 mL PBS per mouse, 5 mice per group) were injected into the tail vein of BALB/c nude mice, respectively. After 7 weeks, all mice were killed by cervical dislocation in a biological safety cabinet (Sujingantai Biotechnology) and the pulmonary metastases were collected for further analysis.

To assess cell metastatic potential, A375-sgNOL7 cells (3×10^6 cells in 0.1 mL PBS per mouse, 5 mice per group) were injected into tail veins of BALB/C nude mice. Mice injected with A375-control cells (3×10^6 cells in 0.1 mL PBS per mouse, 5 mice per group) were used as control group. After 7 weeks, all mice were sacrificed by cervical dislocation and dissected in a biological safety cabinet. The pulmonary metastatic nodules were counted for further analysis.

To assess the cell tumorigenicity, A375-sgNOL7 cells (6×10^6 cells in 0.1 mL PBS per mouse, 5 mice per group) were subcutaneously injected into the left axillae of BALB/C nude mice. Mice injected with A375-control cells (6×10^6 cells in 0.1 mL per mouse, 5 mice per group) were used as control group. About 7-10 days later, the subcutaneous tumor grew and tumor volumes were measured every alternate day. After 4 weeks, all mice were killed by cervical dislocation and dissected in a biological safety cabinet. The tumors were collected for further analysis.

Pathological analysis

Excised neoplasms and lung tissues were embedded in paraffin and sliced into sections at thickness of 5 μm . Afterward, histological slices were subjected to hematoxylin and eosin (H&E) staining and imaged by a light microscope (Zeiss).

Immunohistochemistry (IHC)

For validation of the clinical significance of NOL7 in melanoma. Various clinical samples from melanoma patients (normal skin, n = 5; nevus, n = 5; primary melanoma, n = 32; metastases, n = 10) were purchased from Shanghai Zhuoli Biotechnology Co., Ltd (Shanghai, China). NOL7 expression in these samples was evaluated by IHC analysis with the assistance of Shanghai Zhuoli Biotechnology Co., Ltd. The immunostaining score of NOL7 in tumor tissues was quantified by the H-score (histochemical score) based on the staining intensity and heterogeneity under a Nano Zoomer S210 (Hamamatsu, Japan). The percentage of immunostaining and the staining intensity were scored as 0, negative; 1, weak; 2, moderate; and 3, strong. H-score was calculated using the following formula:

$$\text{H score} = (\text{percentage of cells of weak intensity} \times 1) + (\text{percentage of cells of moderate intensity} \times 2) + (\text{percentage of cells of strong intensity} \times 3)$$

For analysis of NOL7 expression in melanoma formed in mice. NOL7 expression was evaluated by IHC analysis with the assistance of Wuhan Servicebio Co., Ltd. In brief, paraffin embedded sections were fixed in formaldehyde, and a heat-mediated antigen retrieval step in citrate buffer was performed. The samples were blocked in BSA solution for 2 h at 37°C and incubated with anti-NOL7 antibody overnight at 4°C. An horserdich peroxidase conjugated goat anti-rabbit antibody was used as the secondary antibody. NOL7 protein was visualized by AEC staining and examined under the confocal fluorescence microscope (Nikon Eclipse C1, Nikon).

Statistical analysis

Date for all experiments was managed using GraphPad Prism software 5.0 and represented as the mean \pm s.d. A paired t test was used for two group comparison, and a one-way ANOVA was used for multiple group comparison. $P < 0.05$ was considered representative of a significant difference and statistical significance was symbolized by asterisks corresponding to * $P < 0.05$, ** $P < 0.01$ and *** $P < 0.001$.

Results

NOL7 expression correlates with melanoma progression

Post-metastatic cell lines possess an inherently increased capacity for tumorigenesis and metastasis[17]. As described previously, we established the post-metastatic melanoma cell line B16F10M, derived from the pulmonary metastases of the parental pre-metastatic B16F10 cells. The paired cell lines B16F10 and B16F10M were used to probe the global proteomics signature that marks melanoma metastasis to the lung and secondary tumor growth through iTRAQ screening [14]. The iTRAQ analysis showed that NOL7 was upregulated in B16F10M cells compared to B16F10 cells (Fig. 1A). Similarly, another post-metastatic cell line A375M was derived from the pulmonary metastases of the parental pre-metastatic A375 cells (Fig. 1B). In both metastatic cell lines, we confirmed the increased expression of NOL7 and PCNA

(Proliferating cell nuclear antigen) both at the transcriptional and translational levels, compared with that in the parental B16F10 and A375 cells (Fig. 1C-D).

To further explore the role of NOL7 in melanoma progression, we examined the expression of NOL7 in clinical melanoma samples. Various tissue samples including normal skin, nevus, primary melanoma and melanoma metastases were used. As shown in Fig. 1E, NOL7 expression was nearly undetected in normal skin and nevus samples. In contrast, NOL7 expression was markedly elevated in primary melanoma, and further increased in metastatic melanoma samples. Cumulatively, these findings demonstrate by multiple means that NOL7 is increased in melanoma metastases. As the primary tumors also show augmented levels of NOL7 as compared with the normal skin or healthy nevus, NOL7 might be expected to additionally regulate other malignant characteristics in melanoma. These observations prompted us to sequentially investigate the effects of NOL7 on multiple melanoma activities, from proliferation to *in vivo* metastasis, as detailed in the subsequent sections.

NOL7 knockdown suppresses melanoma cell proliferation and induces cell cycle arrest *in vitro*

As the first step to investigate sequentially the roles NOL7 plays in melanoma progression, we investigated whether NOL7 was required for malignant cell proliferation of melanoma *in vitro* by specific siRNAs knockdown in B16F10 and A375 cells (B16F10-siNOL7 and A375-siNOL7 cells). After siRNA treatment, NOL7 protein expression was barely detectable, and its mRNA levels were decreased by ca.80% and ca.70% in the two cell lines, respectively, compared with control B16F10 and A375 cells, where siRNAs whose sequences did not react on any known genes were transfected (see Methods, Fig. 2A).

With this approach, we observed that NOL7 knockdown significantly reduced the cell proliferation rate and the number of cell colonies, compared with the control group (Fig. 2B-D). Since melanogenesis is a marker of differentiated melanoma cells[18], we examined whether NOL7 knockdown interfered the melanin production in melanoma cells. As shown in **Supplementary Fig. 1**, NOL7 knockdown disrupted melanin biosynthesis and the activity of tyrosinase (enzyme catalyzing the initial rate-limiting reaction in melanin biosynthesis in B16F10 cells[19]).

We next used flow cytometry to assess the involvement of NOL7 in the cell cycle progression. As shown in Fig. 2F, NOL7 knockdown markedly added the cell populations at the S-phase, but reduced the cell populations at the G0/G1-phase. Furthermore, various cell cycle-related proteins were altered by NOL7 knockdown (Fig. 2E). Specifically, the expression levels of p21 and p27 were significantly increased, and those of CDK2, cyclin A and cyclin E - significantly decreased upon the knockdown of NOL7. These changes in the levels of cell cycle regulators are consistent with the S-phase arrest induced by NOL7 knockdown. Indeed, the CDK inhibitors p27 and p21 exert inhibitory effects on cell cycle progression through inhibition of the G1 cyclin/CDK complexes, such as cyclin A/CDK2 and cyclin E/CDK2[20, 21]. S-phase cell-cycle arrest has been previously described to be induced by up-regulation of p21 and p27, reducing formation of active cyclin E/CDK2 and cyclin A/CDK2 complexes [22, 23, 24, 25]. In contrast,

levels of Rb were not affected by NOL7 knockdown, which agrees with the prior observation that Rb is upstream of NOL7[10].

NOL7 is beneficial to cell survival by regulating apoptosis resistance

We next moved to study the role of NOL7 in apoptosis resistance of melanoma cells when subjected to a disadvantageous microenvironment. For this purpose, B16F10-siNOL7 and A375-siNOL7 cells were treated with paclitaxel. Additionally, A375-siNOL7 cells were placed in suspended culture conditions (loss of anchorage) and FBS-free culture conditions (loss of nutrition). Apoptosis assays consistently indicated a higher apoptotic index in cells with NOL7 knockdown (Fig. 3A, **Supplementary Fig. 2**). The MTT assay showed decreased cell viability upon paclitaxel treatment and IC_{50} values in NOL7-knockdown cells compared with those in control groups (Fig. 3B-C).

Subsequently, we domesticated anoikis-resistant A375 cells in a continuous cycle between the adherent culture and suspended culture conditions. After 3 cycles, suspended A375 cells were almost non-apoptotic (Fig. 3D, **Supplementary Fig. 3**). It suggested that domesticated A375 cells were resistant to anoikis. Interestingly, we found a significant upregulation of NOL7 expression in anoikis-resistant cells, suggesting that that NOL7 was associated with the anoikis resistance (Fig. 3E). Similarly, we put the A375-sgNOL7 cells (see below for the details on the CRISPR/Cas9-mediated NOL7-knockout) in a continuous cycle between the adherent culture and suspended culture conditions. Within the 3rd cycles, A375-sgNOL7 cells showed a significantly higher apoptotic index than the parental A375 cells. It suggested that NOL7 depletion impaired anoikis resistance of melanoma cells (**Supplementary Fig. 3**). Furthermore, NOL7 knockdown inhibited the expression of survivin, but promoted the expression of caspase 3, caspase 9, bad and bax (Fig. 3F, **Supplementary Fig. 4**). Cumulatively, these results suggest the participation of NOL7 in melanoma cell self-adaptation and protection against apoptosis induced by chemotherapy and starvation, and against anoikis.

NOL7 knockdown depresses melanoma aggressiveness *in vitro*

Having demonstrated the importance of NOL7 in melanoma cell proliferation, colony formation, and apoptosis resistance, which are largely characteristics of the primary tumor growth, we then moved to study the functions on NOL7 in metastasis. To start, we utilized the wound healing assay, the transwell assay and the cell-ECM/HPMEC adhesion assay in order to evaluate the impact of NOL7 knockdown on cell motility, migration or invasion, and adhesion abilities in melanoma, respectively. As shown in Fig. 4, control B16F10 and A375 cells were faster to cover the wound area than the NOL7 knockdown cells, indicating that the motility of melanoma cells was inferior upon decreasing the NOL7 levels. In the adhesion assay, NOL7 knockdown inhibited cells adhesion to gelatin matrix and HPMECs. In comparison to control cells, the number of B16F10-siNOL7 and A375-siNOL7 cells adhered to gelatin matrix or HPMEC was reduced by 30–40% (Fig. 4B). Meanwhile, falcon cell culture insert systems were used to monitor the process of melanoma cell migration or invasion (migration through Matrigel). Upon NOL7

knockdown, the migratory capabilities were reduced by ca.80% and ca.50% in B16F10 and A3757 cells, and invasive capabilities were reduced by ca.70% and ca.60% in B16F10 and A375 cells, respectively.

NOL7 depletion represses melanoma growth and metastasis *in vivo*

Further to examine the role of NOL7 on melanoma growth *in vivo*, and to assess an independent means of reducing NOL7 levels, we utilized the CRISPR/Cas9 system to generate a stable NOL7-knockout A375 cell line (A375-sgNOL7 cells). The expression of NOL7 in A375-sgNOL7 cells was heavily depleted (Fig. 5A, **inset**). Separately, we measured the cell proliferation and colony formation capabilities of A375-sgNOL7 cells. Same as in Fig. 2B-D, NOL7 knockout markedly reduced cell proliferation and cell colony formation in A375 cells (**Supplementary Fig. 5**). In addition, the 3D spheroid formation assay was employed to grow cells in a 3D globular cluster to simulate the *in vivo* cancer cell growth. After culturing in equal amounts of complete medium for 10 days, A375-sgNOL7 cells had a significantly smaller cell spheroid diameter than control cells (**Supplementary Fig. 6**).

Next, an orthotopic xenograft nude mouse model was established. A375-sgNOL7 cells and control A375 cells were injected subcutaneously into the left axillae of nude mice. Tumor growth was monitored by measuring tumor volumes every two days. In contrast to mice injected with control cells, which ripened large tumors, all five mice injected with A375-sgNOL7 cells appeared to harbor either noticeably smaller tumors or no tumors at all within 4 weeks (Fig. 5A). Then, we surveyed whether NOL7 depletion repressed melanoma cell metastasis. Paired A375-sgNOL7 cells and control A375 cells were injected into the lateral tail veins of nude mice and evaluated for formation of distant metastasis. The end-point analysis revealed that the five mice injected with the control cells formed 54 to 134 tumor nodules per lung. In contrast, the five mice injected with A375-sgNOL7 cells formed 10 to 26 tumor nodules per lung (Fig. 5B). Three out of five mice injected with control cells were sacrificed in advance because they became underweight within 3 weeks, and notable metastases were observed in other locations - in a sharp contrast with no such metastases induced upon the NOL7 knockout cell injection (Fig. 5C). Also, NOL7 was observed to be associated with the overall survival of mice in this model (Fig. 5D). Pathological analysis confirmed the appearance of tumors from A375-sgNOL7 cells, and IHC staining confirmed essentially undetectable NOL7 expression in A375-sgNOL7 cells (Fig. 5A-B).

NOL7 is induced by HIF-1 α under hypoxia and participates in hypoxia-induced EMT and drug resistance in melanoma

Having determined the importance of NOL7 for multiple aspects of melanoma progression, from tumor cell proliferation to metastasis, we then set to unravel the potential molecular mechanisms behind.

Hypoxia/HIF-1 α signaling inducing target gene expression to promote cancer progression and metastasis has been widely recognized[26, 27]. Therefore, we examined whether the hypoxia/HIF-1 α signaling activated NOL7 expression. Western blotting was used to test the expression of HIF-1 α and NOL7 in A375

cells when exposed to hypoxic conditions (1% O₂) for different durations. HIF-1 α expression was triggered in response to hypoxia at 0.5-1 days, peaked at 2 days, and stable HIF-1 α expression was maintained within 5 days. Remarkably, NOL7 expression was induced by hypoxia with a delay as compared to HIF-1 α , peaking at 2 days, and stable NOL7 expression was maintained within 5 days (Fig. 6A). The delay in NOL7 expression under hypoxia could indicate that NOL7 was induced by HIF-1 α . To test this possibility, we employed YC-1, a chemical compound that accelerates HIF-1 α degradation and blocks HIF-1 α expression, during 2 days-culturing under hypoxic conditions (1% O₂). As a result, the protein levels of NOL7 and HIF-1 α returned to their initial levels (Fig. 6B).

HIF-1 α advances cancer development through conferring drug resistance to cancer cells and stimulating the EMT[28, 29]. To identify the role of NOL7 in the hypoxia/HIF-1 α signaling, A375-sgNOL7 cells and control cells were cultured under hypoxic conditions (1% O₂ for 2 days). As shown in Fig. 6C, D and **Supplementary Fig. 7**, NOL7 knockout has no effect on the morphology of A375 under normoxic condition. However, hypoxic condition motivated the conversion of the non-polar (upon the 2D culturing conditions) epithelial phenotype to the polar mesenchymal phenotype, and altered the EMT-associated protein expression of E-cadherin, N-cadherin, Vimentin and Fibronectin. A375 cells invasion and migration were strikingly enhanced after the hypoxic treatment. Interestingly, NOL7 depletion reversed the hypoxia-induced EMT and impaired the elevated invasion and migration characteristics (Fig. 6E-F).

Furthermore, to investigate the contribution of NOL7 to chemoresistance caused by hypoxia, we inspected the sensitivity of A375-sgNOL7 cells to paclitaxel under hypoxia. As expected, decreased cytotoxicity of paclitaxel and improved IC₅₀ values were observed under hypoxia. Further, NOL7 knockout reverted the hypoxia-induced desensitization of A375 cells to the drug (Fig. 6G-H). Thus, NOL7 is induced by HIF-1 α under hypoxia and is required for HIF-1 α -induced EMT, invasiveness, and chemoresistance.

NOL7 modulates EMT and the PI3K/AKT/ERK pathway in melanoma

To further explore the molecular mechanism(s) of the NOL7-induced melanoma malignancy, we investigated the participation of NOL7 in EMT and the AKT, ERK, JNK, and Wnt/ β -catenin signaling pathways, which are widely recognized as activators of cancer progression[30, 31]. As shown in Fig. 7A, NOL7 knockdown/knockout increased the levels of the epithelial marker E-cadherin, and correspondingly depressed the levels of mesenchymal makers N-cadherin, MMP9, Vimentin and Twist both in B16F10 and A375 cells. Meanwhile, NOL7 knockdown/knockout in B16F10 and A375 cells led to decreased levels of p-AKT and p-ERK, while GSK3 β , a negative regulator of the PI3K/AKT/ERK signaling and Wnt/ β -catenin signaling, was upregulated[32] (Fig. 7B). However, JNK, p-JNK, β -catenin and rhoA levels were unaffected after NOL7 knockout in B16F10 or A375 cells (**Supplementary Fig. 8**). These results indicate that NOL7 modulates EMT and the PI3K/AKT/ERK pathway and, potentially, the Wnt/ β -catenin signaling, to promote melanoma progression. At the same time, we find no impact of modulation of NOL7 levels on such established players in the EMT program as TSP-1, SMAD2/3, and pSMAD2/3[33, 34] (**Supplementary Fig. 9**).

Discussion

Melanoma is one of the most undesirable clinical events, due to its dramatic tendency toward distal metastasis[35, 36]. Over the years, we have focused on uncovering the identity and mechanisms of key molecules that regulate how the few disseminated cancer cells survive and metastasize[17, 37]. In the current study, we identified NOL7, one of the top altered genes from the metastatic melanoma signature, and subjected it to further intensive studies. Herein, we presented that NOL7 is a novel and multifunctional oncogene in melanoma operating in the tumor progression and dissemination mechanisms. These findings contrast with the prior description of NOL7 as a tumor suppressor in cervical cancer[9]. Previous studies have shown that melanoma is commonly associated with an amplification of the chromosome region 6p, particularly 6p21-23 where the NOL7 gene resides, and that this region frequently undergoes heterozygous loss in cervical cancer[38]. It might therefore be predicted that NOL7 exhibits a different expression pattern and plays different roles in melanoma and cervical cancer.

Our data suggest that NOL7 is induced by HIF-1 α to promote melanoma progression, potentially through modulation of the PI3K/AKT/ERK pathway. Hypoxia is a fundamental hallmark of tumor microenvironment, and the hypoxia/HIF-1 α signaling is critical for cancer progression[27]. Previous reports have shown that HIF-1 α can induce many molecules and further activate several downstream signaling pathways, including the PI3K/AKT, ERK and MAPK pathways, to regulate malignant behaviors in cancer cells[39]. We observed that NOL7 expression was stimulated by the hypoxia/HIF-1 α signaling and mediated the HIF-1 α -triggered EMT, cell aggressiveness and chemoresistance (Fig. 6). Numerous published studies have indicated that the PI3K/AKT, ERK, JNK and rhoA signaling pathways are frequently dysregulated in human cancers[40, 41]. Aberrant activation of these pathways leads to extensive cellular transformation, tumorigenesis, disease deterioration and resistance to treatment. Here, we disclosed that NOL7 promoted the AKT and ERK phosphorylation and decreased the GS3K β expression, but had no effect on JNK, p-JNK, β -catenin and rhoA (Fig. 7, **Supplementary Fig. 8**).

Cancer cell growth is associated with acceleration of cell cycle progression and acquisition of apoptotic resistance[42, 43]. As the core components of the cell cycle machinery, cyclins and their catalytic partners cyclin-dependent kinases (CDKs) drive cell cycle progression in cancer cells; on the contrary, CDK inhibitors such as p21 or p27 negatively regulate this process[44, 45]. Furthermore, apoptosis regulatory proteins, such as the pro-apoptotic caspase family proteins and bax maintain the immortality of cancer cells [46, 47]. The PI3K/AKT/ERK pathway has been shown to regulate CDKs, p21, and cyclins to expedite the cell cycle progression, and to alter the expression of caspases proteins to defend against apoptosis, which results in drug resistance[48]. In the current study, we showed that NOL7 depletion altered protein levels of p27, p21, CDK2, cyclin A and cyclin E to induce the S-phase arrest in melanoma cells. Paclitaxel is a chemotherapy drug conventionally applied to melanoma patients in China[49] and drives apoptosis through cell cycle arrest in the G2/M phase[50]. We kept in mind the potential for the synergistic action of the drug on top of the NOL7 knockdown. Data also revealed that NOL7 could decrease the sensitivity of melanoma cells to paclitaxel treatment and to anoikis (Fig. 2–3).

The connection between the PI3K/AKT/ERK pathway and EMT has been well-documented. During EMT, cancer cells change their morphology, extend pseudopodia, degrade the surrounding basement membrane and invade through the ECM. Activation of the PI3K/AKT/ERK pathway leads to EMT through the induction of MMP9 and increased activity of GSK3 β [51]. As observed in the current research, NOL7 promoted the PI3K/AKT/ERK pathway and induced EMT to improve the metastatic potential of melanoma cells. Importantly, the observation that depletion of NOL7 reversed the EMT and arrested the cell cycle, as well as opposed chemoresistance and metastasis is consistent with the data on the role of NOL7 in the hypoxia/HIF-1 α signaling. Collectively, these data depict the molecular mechanism whereby the hypoxia/HIF-1 α signaling induces NOL7 expression to further govern the revitalization of the PI3K/AKT/ERK pathway.

Conclusion

Taken together, our research reveals the crucial role of NOL7 in melanoma. From a functional perspective, NOL7 is beneficial for cell survival and contributes to tumor growth and metastasis of melanoma through promoting cell proliferation, cell cycle progression, aggressiveness, as well as acquisition of chemo- and anoikis-resistance. From a mechanistic perspective, NOL7 emerges as a novel player within the HIF-1 α /PI3K/AKT/ERK axis to ultimately activate regulators of the cell cycle, apoptosis and EMT to exert its oncogenic function.

In summary, we identify NOL7 as a multifunctional regulator of malignant activities, proposing it as a novel biomarker of melanoma progression and potential drug target for future therapeutics.

Abbreviations

NOL7: nucleolar protein 7; CRISPR: clustered regularly interspaced short Palindromic repeats; HIF: hypoxia inducible factor; ECM: extracellular matrix; STR: short tandem repeat; IHC: Immunohistochemistry; iTRAQ: isobaric tags for relative and absolute quantification; FBS: fetal bovine serum; PBS: phosphate buffer saline; EMT: epithelial mesenchymal transition; CDK: cyclin-dependent kinase; MMP: matrix metalloprotein; PI: propidium iodide; FITC: fluorescein isothiocyanate.

Declarations

Ethics approval and consent to participate

The animal experimental procedures are in compliance with the guiding principles and approved by Institutional Animal Care and Use Committee of Fuzhou University. The approval number is SYXK-2019-0007.

Consent for publication

Not applicable.

Availability of data and materials

All data generated or analysed during this study are included in this published article and its supplementary information files.

Competing interests

No potential conflicts of interest are disclosed.

Funding:

This work was supported by the grants from National Natural Science Foundation of China (81961138017, 81773063, U1505225) and Ministry of Science and Technology of China (2015CB931804).

Authors' contributions

L. J, L. K and YM. L conceived and designed this research; YM. L, L. J and V. L. K wrote and revised this manuscript; YM. L, F. C, WY. S, BF. L, N. Z and YS. L performed and validated the experiments. YM. L and F. C managed data and drew the pictures; L. J and V. L. K supervised this study.

Acknowledgments

Not applicable.

References

1. Eggermont AM, Spatz A, Robert C. Cutaneous melanoma. *Lancet*. 2014;383:816–27.
2. Hodis E, Watson IR, Kryukov GV, Arold ST, Imielinski M, Theurillat J, et al. A Landscape of Driver Mutations in Melanoma. *Cell*. 2012;150:251–63.
3. Obenauf AC, Massague J. Surviving at a distance: organ specific metastasis. *Trends Cancer*. 2015;1:76–91.
4. Ossio R, Roldán-Marín R, Martínez-Said H, Adams DJ. C.D. Robles-Espinoza, Melanoma: a global perspective. *Nat Rev Cancer*. 2017;17:393–4.
5. de Groot AE, Roy S, Brown JS, Pienta KJ, Amend SR. Revisiting Seed and Soil: Examining the Primary Tumor and Cancer Cell Foraging in Metastasis. *Mol Cancer Res*. 2017;15:361–70.
6. Owens B. Melanoma *Nature*. 2014;515:109.
7. Castello A, Fischer B, Eichelbaum K, Horos R, Beckmann BM, Strein C, et al. Insights into RNA biology from an atlas of mammalian mRNA-binding proteins. *Cell*. 2012;149:1393–406.

8. Zhou G, Colleen LD, Mark WL. Identification and functional analysis of NOL7 nuclear and nucleolar localization signals. *BMC Cell Biology* 11 (2010).
9. Hasina R, Pontier AL, Fekete MJ, Martin LE, Qi XM, Brigaudeau C, et al. NOL7 is a nucleolar candidate tumor suppressor gene in cervical cancer that modulates the angiogenic phenotype. *Oncogene*. 2006;25:588–98.
10. Mankame TP, Lingen MW. The RB tumor suppressor positively regulates transcription of the anti-angiogenic protein NOL7. *Neoplasia*. 2012;14:1213–22.
11. Mankame TP, Zhou G, Lingen MW. Identification and characterization of the human NOL7 gene promoter. *Gene*. 2010;456:36–44.
12. Kinor N, Shav-Tal Y. The dynamics of the alternatively spliced NOL7 gene products and role in nucleolar architecture. *Nucleus-Phila*. 2011;2:229–45.
13. Khanna C. Modeling metastasis in vivo. *Carcinogenesis*. 2004;26:513–23.
14. Li Y, Zhou Y, Li B, Chen F, Shen W, Lu Y, et al. WDR74 modulates melanoma tumorigenesis and metastasis through the RPL5–MDM2–p53 pathway. *Oncogene*. 2020;39:2741–55.
15. Ran FA, Hsu PD, Wright J, Agarwala V, Scott DA, Zhang F. Genome engineering using the CRISPR-Cas9 system. *Nat Protoc*. 2013;8:2281–308.
16. Guo YQ, Ding Y, Li DD, Li JJ, Peng RQ, Wen XZ, et al. Efficacy and safety of nab-paclitaxel combined with carboplatin in Chinese patients with melanoma. *Med Oncol*. 2015;32:234.
17. Li B, Shen W, Peng H, Li Y, Chen F, Zheng L, et al. Fibronectin 1 promotes melanoma proliferation and metastasis by inhibiting apoptosis and regulating EMT. *Onco Targets Ther*. 2019;12:3207–21.
18. Kageyama A, Oka M, Okada T, Nakamura S, Ueyama T, Saito N, et al. Down-regulation of melanogenesis by phospholipase D2 through ubiquitin proteasome-mediated degradation of tyrosinase. *J Biol Chem*. 2004;279:27774–80.
19. Hearing VJ. Biochemical control of melanogenesis and melanosomal organization. *J Investig Dermatol Symp Proc*. 1999;4:24–8.
20. Adams JM, Cory S. The Bcl-2 apoptotic switch in cancer development and therapy. *Oncogene*. 2007;26:1324–37.
21. Polyak K, Lee MH, Erdjument-Bromage H, Koff A, Roberts JM, Tempst P, et al. Cloning of p27Kip1, a cyclin-dependent kinase inhibitor and a potential mediator of extracellular antimitogenic signals. *Cell*. 1994;78:59–66.
22. Huang Z, Wang L, Chen L, Zhang Y, Shi P. Induction of cell cycle arrest via the p21, p27-cyclin E,A/Cdk2 pathway in SMMC-7721 hepatoma cells by clioquinol. *Acta Pharm*. 2015;65:463–71.
23. Karimian H, Arya A, Fadaeinasab M, Razavi M, Hajrezaei M, Karim KA, et al. *Kelussia odoratissima* Mozaff. activates intrinsic pathway of apoptosis in breast cancer cells associated with S phase cell cycle arrest via involvement of p21/p27 in vitro and in vivo. *Drug Des Devel Ther*. 2017;11:337–50.
24. Yeo EJ, Ryu JH, Chun YS, Cho YS, Jang IJ, Cho H, et al. YC-1 induces S cell cycle arrest and apoptosis by activating checkpoint kinases. *Cancer Res*. 2006;66:6345–52.

25. Sancar A, Lindsey-Boltz LA, Unsal-Kacmaz K, Linn S. Molecular mechanisms of mammalian DNA repair and the DNA damage checkpoints. *Annu Rev Biochem.* 2004;73:39–85.
26. Loftus SK, Baxter LL, Cronin JC, Fufa TD, Pavan WJ. Hypoxia-induced HIF1 α targets in melanocytes reveal a molecular profile associated with poor melanoma prognosis. *Pigm Cell Melanoma R.* 2017;30:339–52.
27. Ackerman D, Simon MC. Hypoxia, lipids, and cancer: surviving the harsh tumor microenvironment. *Trends Cell Biol.* 2014;24:472–8.
28. Gilkes DM, Semenza GL, Wirtz D. Hypoxia and the extracellular matrix: drivers of tumour metastasis. *Nat Rev Cancer.* 2014;14:430–9.
29. Rohwer N, Cramer T. Hypoxia-mediated drug resistance: novel insights on the functional interaction of HIFs and cell death pathways. *Drug Resist Updat.* 2011;14:191–201.
30. Papa S, Choy PM, Bubici C. The ERK and JNK pathways in the regulation of metabolic reprogramming. *Oncogene.* 2019;38:2223–40.
31. Blagodatski A, Poteryaev D, Katanaev VL. Targeting the Wnt pathways for therapies. *Mol Cell Ther.* 2014;2:28.
32. Mayer IA, Arteaga CL. The PI3K AKT Pathway as a Target for Cancer Treatment. *Annu Rev Med.* 2016;67:11–28.
33. Yeh HW, Hsu EC, Lee SS, Lang YD, Lin YC, Chang CY, et al. PSPC1 mediates TGF- β 1 autocrine signalling and Smad2/3 target switching to promote EMT, stemness and metastasis. *Nat Cell Biol.* 2018;20:479–91.
34. Jayachandran A, Anaka M, Prithviraj P, Hudson C, McKeown SJ, Lo PH, et al. Thrombospondin 1 promotes an aggressive phenotype through epithelial-to-mesenchymal transition in human melanoma. *Oncotarget.* 2014;5:5782–97.
35. Miller AJ, Mihm MJ. Melanoma *N Engl J Med.* 2006;355:51–65.
36. Clark WJ, Elder DE, Guerry DT, Epstein MN, Greene MH, Van Horn M. A study of tumor progression: the precursor lesions of superficial spreading and nodular melanoma. *Hum Pathol.* 1984;15:1147–65.
37. Shen W, Li Y, Li B, Zheng L, Xie X, Le J, et al. Downregulation of KCTD12 contributes to melanoma stemness by modulating CD271. *Cancer Biol Med.* 2019;16:498–513.
38. Dou C, Zhou Z, Xu Q, Liu Z, Zeng Y, Wang Y, et al. Hypoxia-induced TUFT1 promotes the growth and metastasis of hepatocellular carcinoma by activating the Ca²⁺/PI3K/AKT pathway. *Oncogene.* 2019;38:1239–55.
39. Papa S, Choy PM, Bubici C. The ERK and JNK pathways in the regulation of metabolic reprogramming. *Oncogene.* 2019;38:2223–40.
40. Acharya BR, Nestor-Bergmann A, Liang X, Gupta S, Duszyc K, Gauquelin E, et al. A Mechanosensitive RhoA Pathway that Protects Epithelia against Acute Tensile Stress. *Dev Cell.* 2018;47:439–52.e6.

41. Su Z, Yang Z, Xu Y, Chen Y, Yu Q. Apoptosis, autophagy, necroptosis, and cancer metastasis. *Mol Cancer*. 2015;14:48.
42. Pencheva N, Buss CG, Posada J, Merghoub T, Tavazoie SF. Broad-Spectrum Therapeutic Suppression of Metastatic Melanoma through Nuclear Hormone Receptor Activation. *Cell*. 2014;156:986–1001.
43. Zerjatke T, Gak IA, Kirova D, Fuhrmann M, Daniel K, Gonciarz M, et al. Quantitative Cell Cycle Analysis Based on an Endogenous All-in-One Reporter for Cell Tracking and Classification. *Cell Rep*. 2017;19:1953–66.
44. Law M, Forrester E, Chytil A, Corsino P, Green G, Davis B, et al. Rapamycin disrupts cyclin/cyclin-dependent kinase/p21/proliferating cell nuclear antigen complexes and cyclin D1 reverses rapamycin action by stabilizing these complexes. *Cancer Res*. 2006;66:1070–80.
45. McIlwain DR, Berger T, Mak TW. Caspase Functions in Cell Death and Disease. *Csh Perspect Biol*. 2013;5:a008656–6.
46. Delbridge AR, Grabow S, Strasser A, Vaux DL. Thirty years of BCL-2: translating cell death discoveries into novel cancer therapies. *Nat Rev Cancer*. 2016;16:99–109.
47. Hsieh MJ, Tsai TL, Hsieh YS, Wang CJ, Chiou HL. Dioscin-induced autophagy mitigates cell apoptosis through modulation of PI3K/Akt and ERK and JNK signaling pathways in human lung cancer cell lines. *Arch Toxicol*. 2013;87:1927–37.
48. Chinese guidelines for diagnosis and treatment of melanoma 2019 (Chinese version). CSCO. Beijing, People's Medical Publishing House, 2019, 61–130 *Chin J Cancer Res* 31 (2019) 578–585.
49. Das GC, Holiday D, Gallardo R, Haas C. Taxol-induced cell cycle arrest and apoptosis: dose-response relationship in lung cancer cells of different wild-type p53 status and under isogenic condition. *Cancer Lett*. 2001;165:147–53.
50. Niederst MJ, Benes CH. EMT twists the road to PI3K. *Cancer Discov*. 2014;4:149–51.

Figures

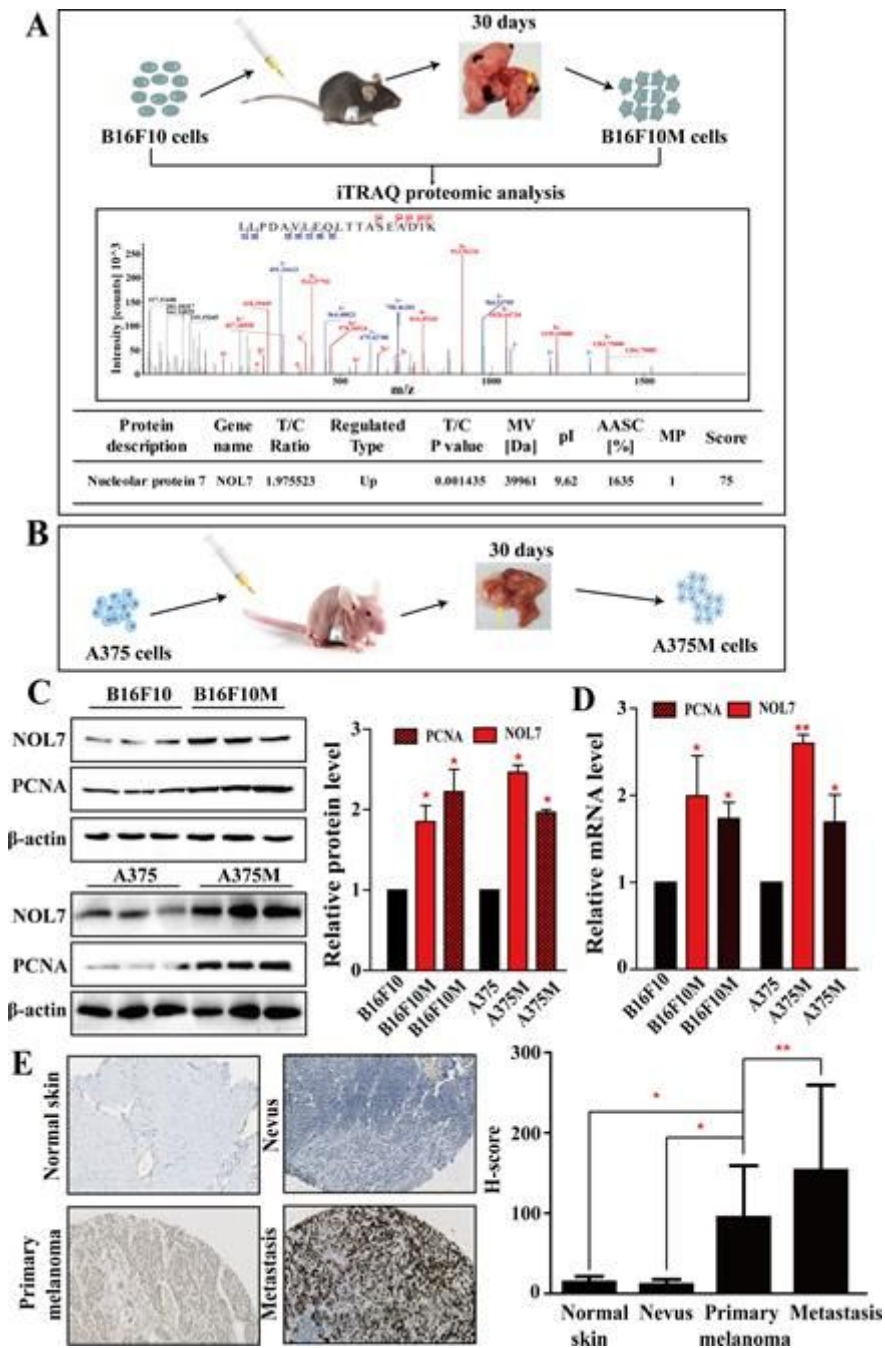


Figure 1

NOL7 expression is upregulated in primary and metastatic melanoma. A. Flow chart illustrates the establishment of post-metastatic melanoma cell line, B16F10M. Post-metastatic melanoma cell line, B16F10M was derived from pro-metastatic melanoma cells, B16F10 through an animal model of hematogenous tumor metastasis. Global proteomic alterations between B16F10 and B16F10M cells were identified by iTRAQ[14]. Furthermore, mass spectrum peaks for a unique peptide fragment pertaining to NOL7 protein and identification outcomes of NOL7 protein among B16F10 (sample ID: C) and B16F10M (sample ID: T) are shown below. B. A Flow chart shows the establishment of post-metastatic melanoma cell line, A375M derived from pro-metastatic melanoma cells, A375 through an animal model of hematogenous tumor metastasis. C-D. Increased protein expression level of NOL7 and PCNA in B16F10M

and A375M cells relative to B16F10 and A375 cells, respectively, as measured by western blotting and qRT-PCR. Black columns represent that the levels of PCNA and NOL7 expression in B16F10 and A375 cells were normalized to 1. β -actin was served as the internal control. E. NOL7 expression was increased in the disease progression from normal skin and nevus to primary melanoma and further to metastatic melanoma as detected by IHC analysis. The H-score for quantification of NOL7 expression was shown in right.

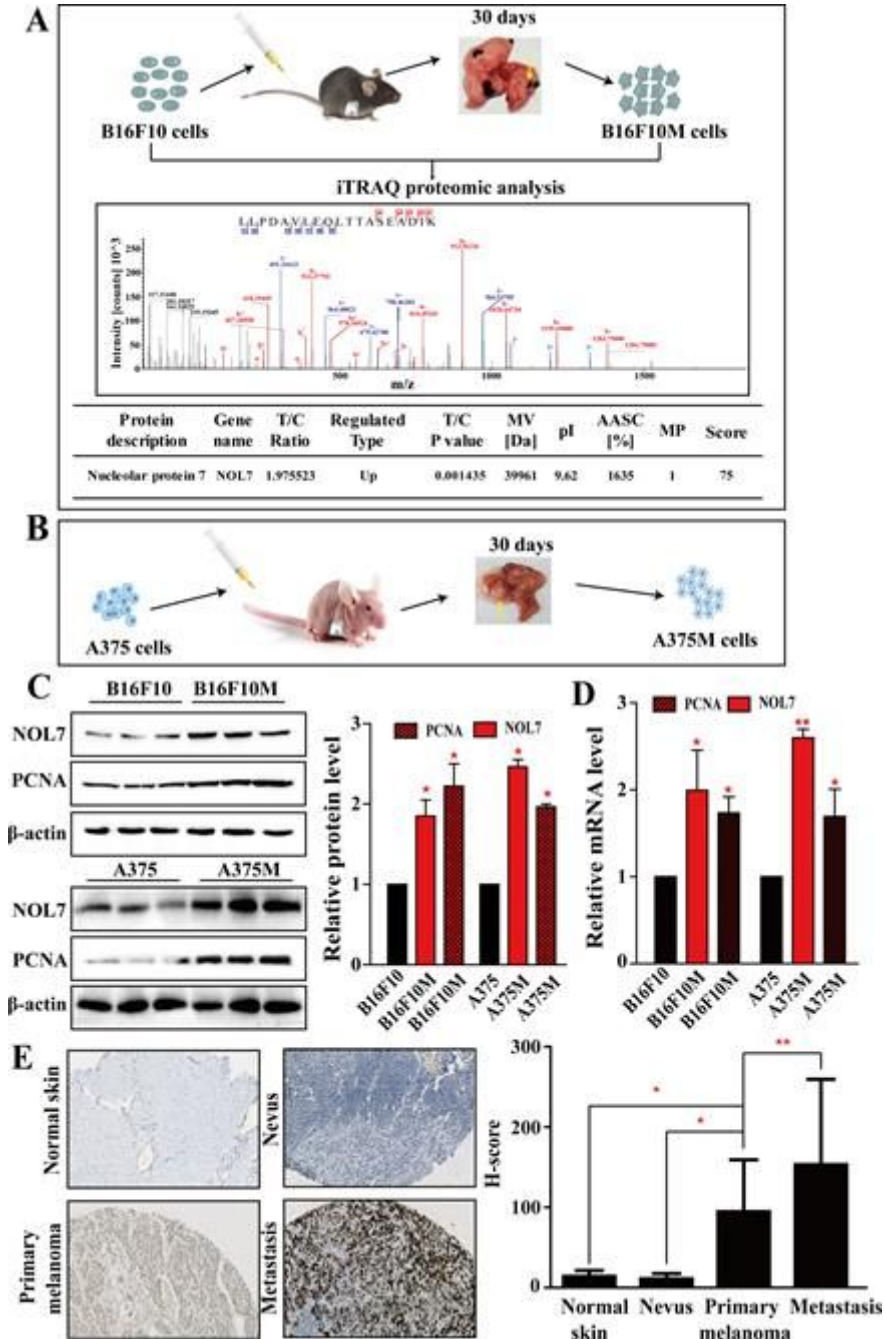


Figure 1

NOL7 expression is upregulated in primary and metastatic melanoma. A. Flow chart illustrates the establishment of post-metastatic melanoma cell line, B16F10M. Post-metastatic melanoma cell line, B16F10M was derived from pro-metastatic melanoma cells, B16F10 through an animal model of

hematogenous tumor metastasis. Global proteomic alterations between B16F10 and B16F10M cells were identified by iTRAQ[14]. Furthermore, mass spectrum peaks for a unique peptide fragment pertaining to NOL7 protein and identification outcomes of NOL7 protein among B16F10 (sample ID: C) and B16F10M (sample ID: T) are shown below. B. A Flow chart shows the establishment of post-metastatic melanoma cell line, A375M derived from pro-metastatic melanoma cells, A375 through an animal model of hematogenous tumor metastasis. C-D. Increased protein expression level of NOL7 and PCNA in B16F10M and A375M cells relative to B16F10 and A375 cells, respectively, as measured by western blotting and qRT-PCR. Black columns represent that the levels of PCNA and NOL7 expression in B16F10 and A375 cells were normalized to 1. β -actin was served as the internal control. E. NOL7 expression was increased in the disease progression from normal skin and nevus to primary melanoma and further to metastatic melanoma as detected by IHC analysis. The H-score for quantification of NOL7 expression was shown in right.

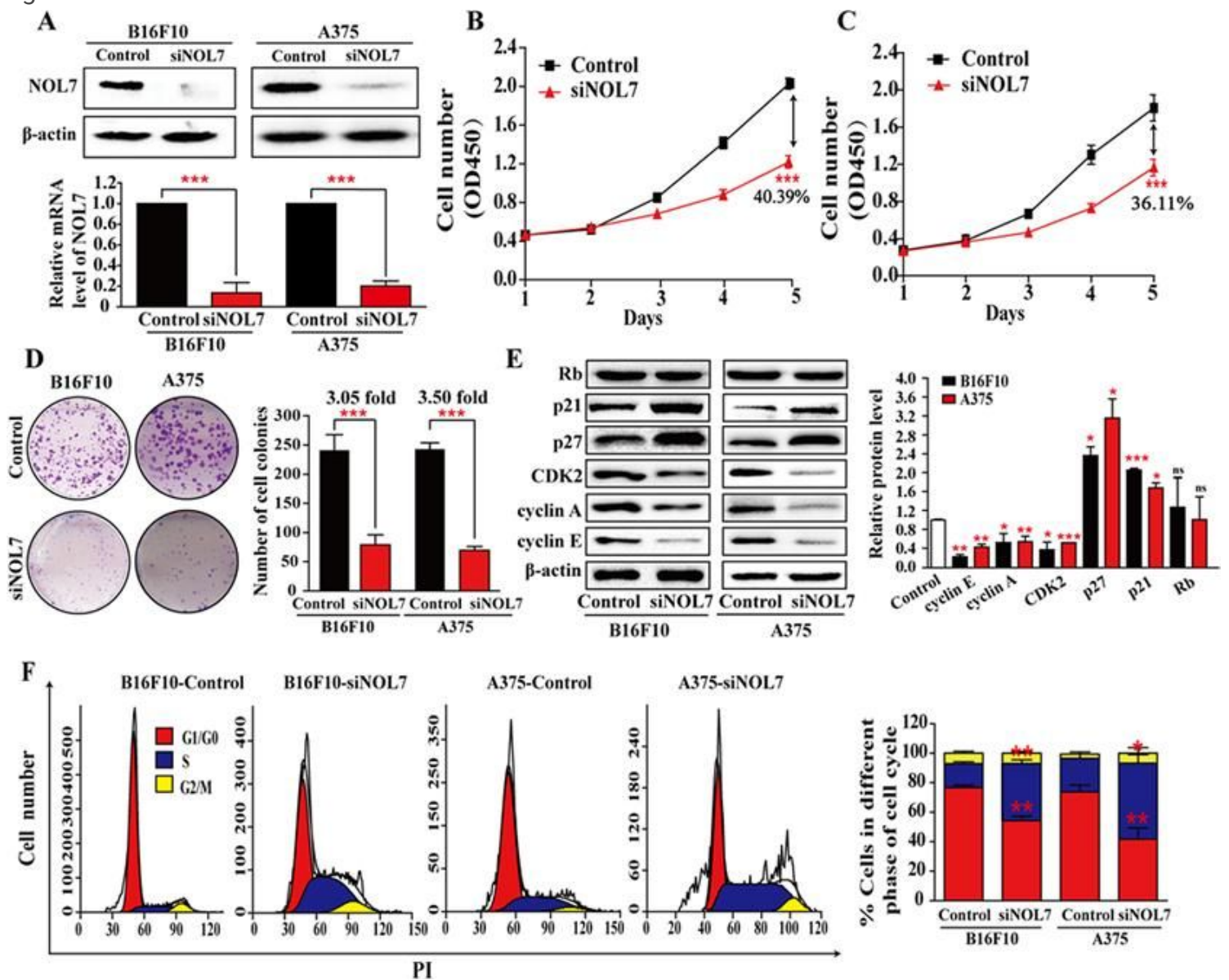


Figure 2

NOL7 knockdown suppresses cell proliferation and induces cell cycle S phase arrest in melanoma cells. A. Success in NOL7-knockdown in B16F10 and A375 cells by siNOL7. B-D. Lower cell proliferation and decreased cell colony formation on 14th day upon NOL7-knockdown in B16F10 and A375 cells. E. Effect of NOL7 knockdown on cell cycle-associated proteins. NOL7 knockdown decreased the expression level of cyclin A, cyclin E, CDK2 and enhanced the expression level of p21 and p27 in B16F10 and A375 cells. The quantification of these proteins was shown in right F. Flow cytometry scans and the quantitative analysis shows higher proportion of S phase population upon NOL7 knockdown in B16F10 and A375 cells. Data are means \pm s.d., for each cohort, $n \geq 3$; *, $P < 0.05$, **, $P < 0.01$, ***, $P < 0.001$; t-test.

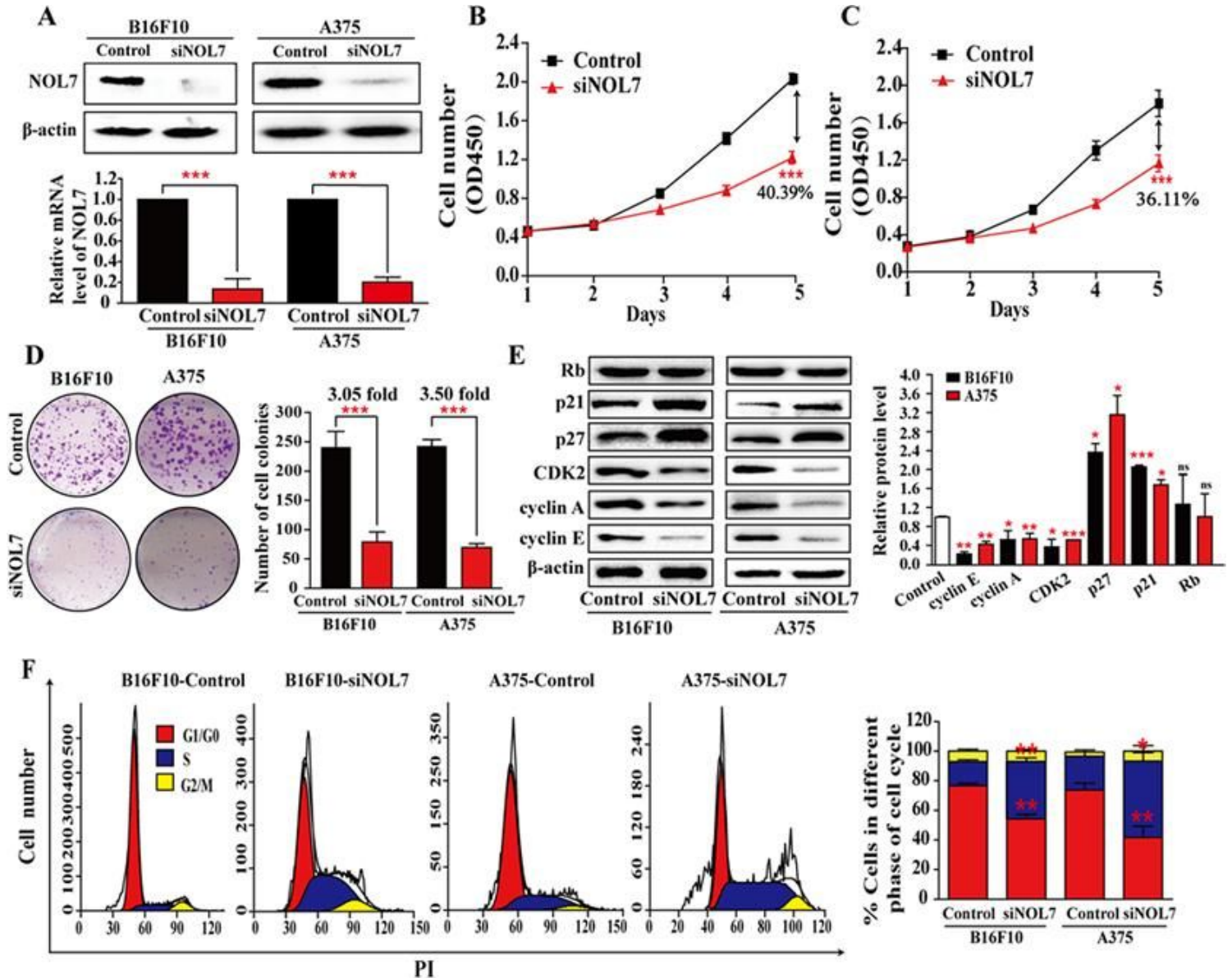


Figure 2

NOL7 knockdown suppresses cell proliferation and induces cell cycle S phase arrest in melanoma cells. A. Success in NOL7-knockdown in B16F10 and A375 cells by siNOL7. B-D. Lower cell proliferation and decreased cell colony formation on 14th day upon NOL7-knockdown in B16F10 and A375 cells. E. Effect of NOL7 knockdown on cell cycle-associated proteins. NOL7 knockdown decreased the expression level

of cyclin A, cyclin E, CDK2 and enhanced the expression level of p21 and p27 in B16F10 and A375 cells. The quantification of these proteins was shown in right F. Flow cytometry scans and the quantitative analysis shows higher proportion of S phase population upon NOL7 knockdown in B16F10 and A375 cells. Data are means \pm s.d., for each cohort, $n \geq 3$; *, $P < 0.05$, **, $P < 0.01$, ***, $P < 0.001$; t-test.

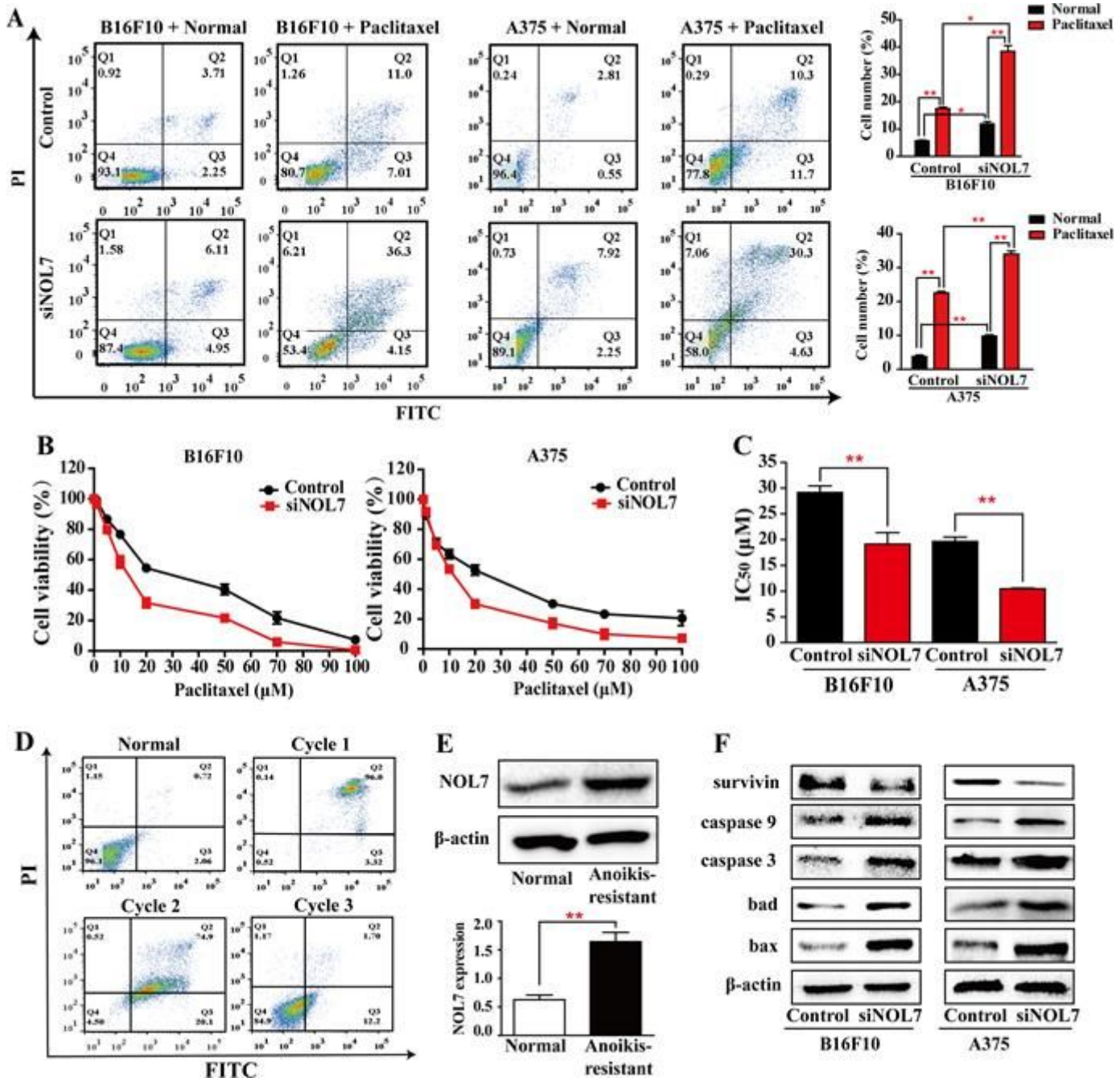


Figure 3

NOL7 is associated with lower sensitivity to paclitaxel and anoikis resistance in melanoma cells. A-C. NOL7 knockdown increased sensitivity of B16F10 and A375 cells to paclitaxel. Target cells were incubated with paclitaxel at various concentration for 24 h and cell viability was tested by MTT assay. In addition, target cells were incubated with 10 μM paclitaxel for 24 h and apoptotic cells were analyzed by Annexin V-FITC/PI staining kit using flow cytometry. D-E. Flow cytometry scans show the generation of

anoikis-resistant A375 cells and western blotting shows the upregulation of NOL7 expression in anoikis-resistant A375 cells as compared to normal A375 cells. F. Western blotting revealed the alteration of apoptosis-related proteins expression upon NOL7 knockdown in B16F10 and A375 cells. Quantification of these proteins was shown in supplementary Fig. 4. Data are mean \pm s.d. ($n \geq 3$); *, $P < 0.05$, **, $P < 0.01$, t-test.

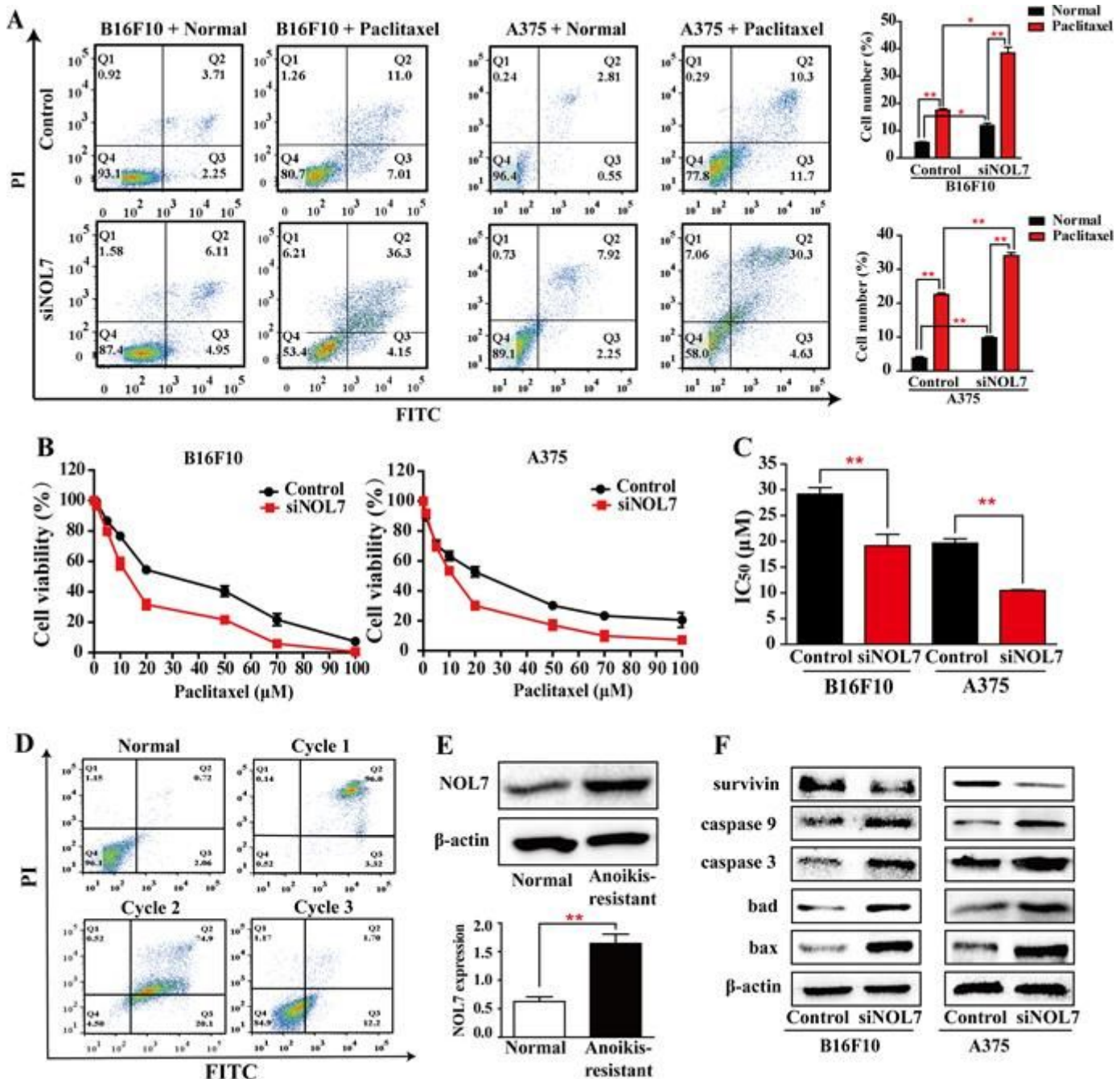


Figure 3

NOL7 is associated with lower sensitivity to paclitaxel and anoikis resistance in melanoma cells. A-C. NOL7 knockdown increased sensitivity of B16F10 and A375 cells to paclitaxel. Target cells were incubated with paclitaxel at various concentration for 24 h and cell viability was tested by MTT assay. In addition, target cells were incubated with 10 μ M paclitaxel for 24 h and apoptotic cells were analyzed by

Annexin V-FITC/PI staining kit using flow cytometry. D-E. Flow cytometry scans show the generation of anoikis-resistant A375 cells and western blotting shows the upregulation of NOL7 expression in anoikis-resistant A375 cells as compared to normal A375 cells. F. Western blotting revealed the alteration of apoptosis-related proteins expression upon NOL7 knockdown in B16F10 and A375 cells. Quantification of these proteins was shown in supplementary Fig. 4. Data are mean \pm s.d. ($n \geq 3$); *, $P < 0.05$, **, $P < 0.01$, t-test.

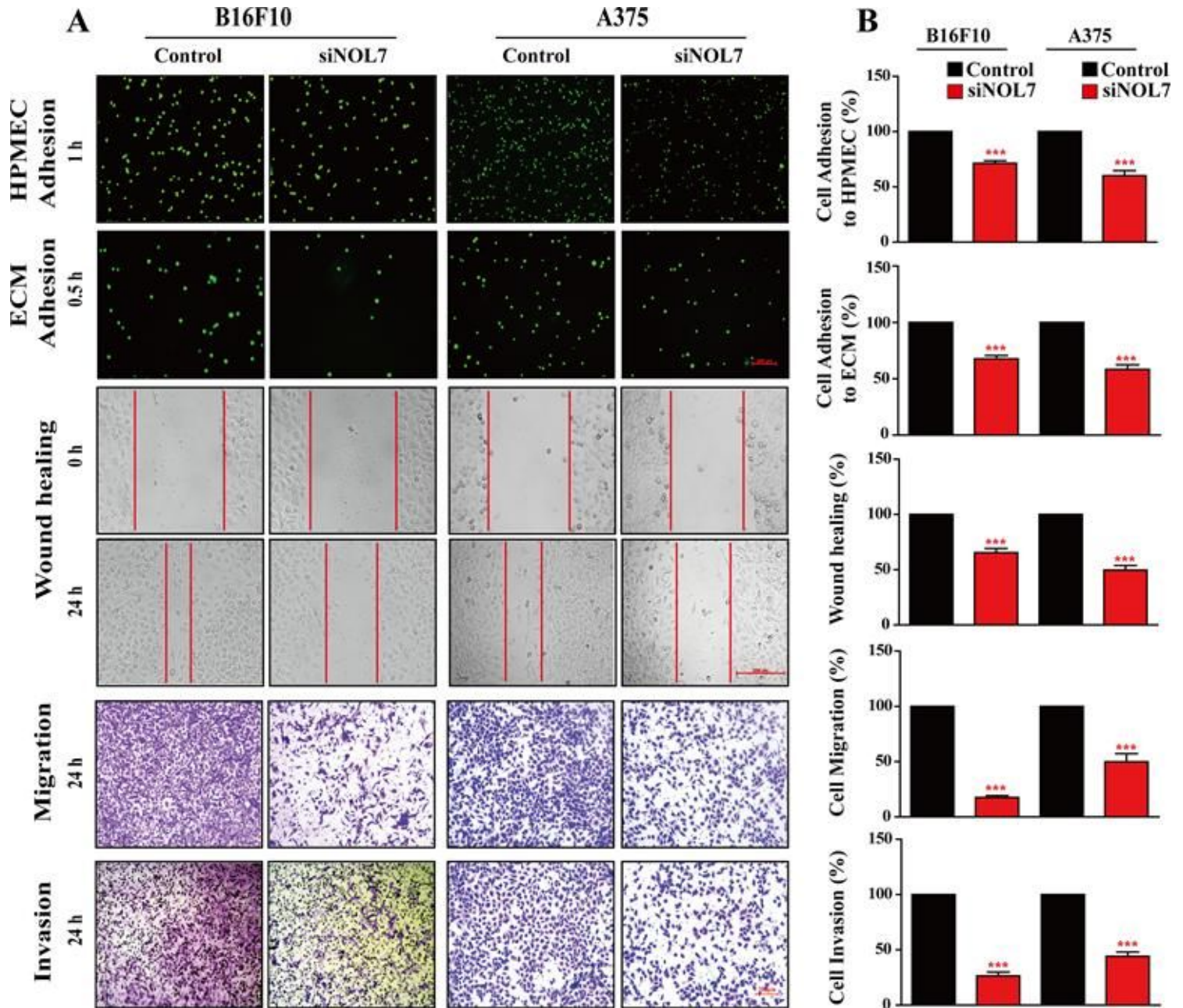


Figure 4

NOL7 correlates with metastatic potential of melanoma cells. A. Phase micrograph showing adherent melanoma cells (above), melanoma cells during wound healing (middle) and migrating and invading (below) melanoma cells at different time intervals after NOL7 knockdown. B. Quantitative analysis of the

effect of NOL7 knockdown on cell adhesion, cell motility, cell migration and cell invasion of B16F10 and A375 cells. Data are mean \pm s.d. ($n \geq 3$); *, $P < 0.05$, **, $P < 0.01$, ***, $P < 0.001$, t-test.

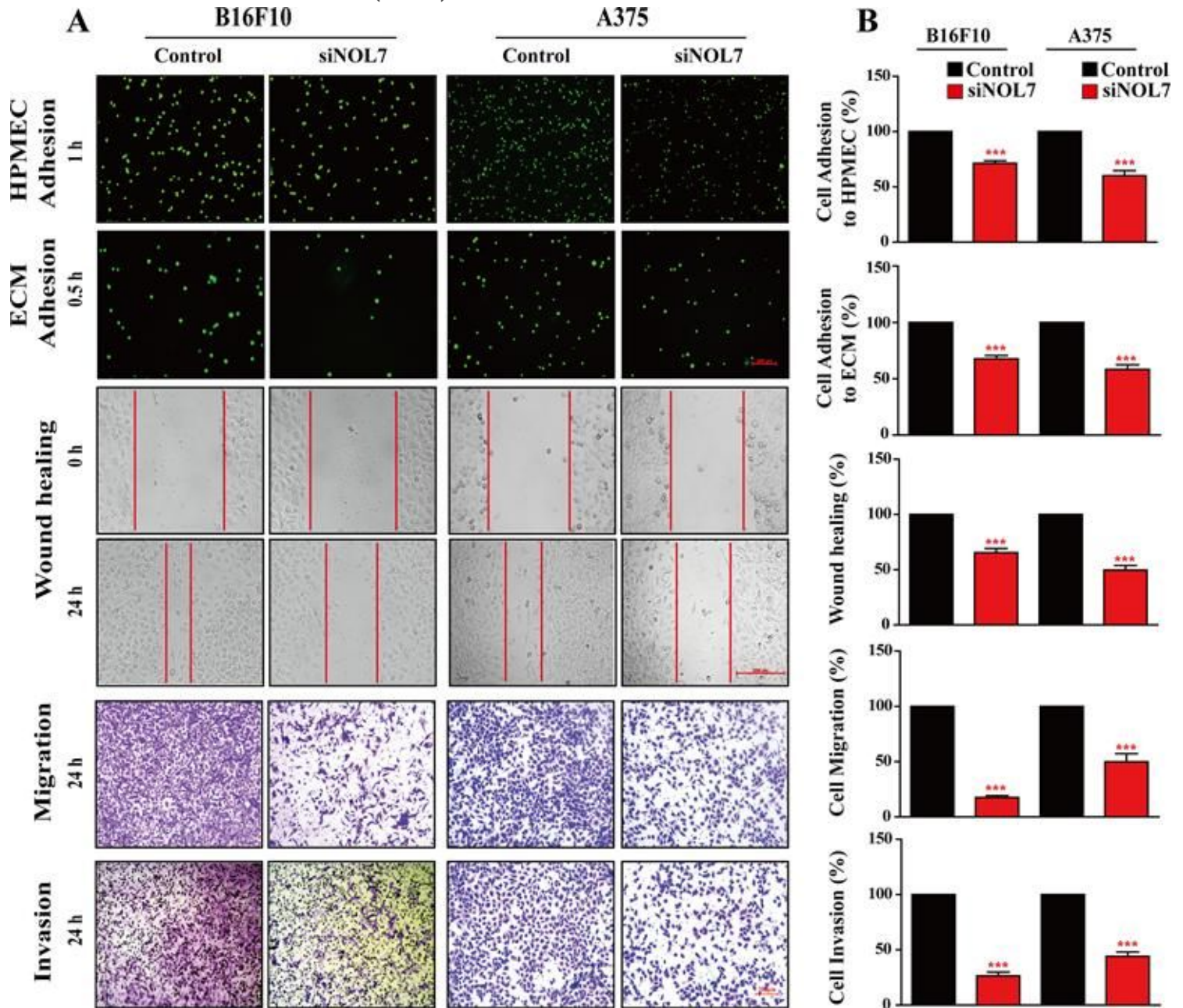


Figure 4

NOL7 correlates with metastatic potential of melanoma cells. A. Phase micrograph showing adherent melanoma cells (above), melanoma cells during wound healing (middle) and migrating and invading (below) melanoma cells at different time intervals after NOL7 knockdown. B. Quantitative analysis of the effect of NOL7 knockdown on cell adhesion, cell motility, cell migration and cell invasion of B16F10 and A375 cells. Data are mean \pm s.d. ($n \geq 3$); *, $P < 0.05$, **, $P < 0.01$, ***, $P < 0.001$, t-test.

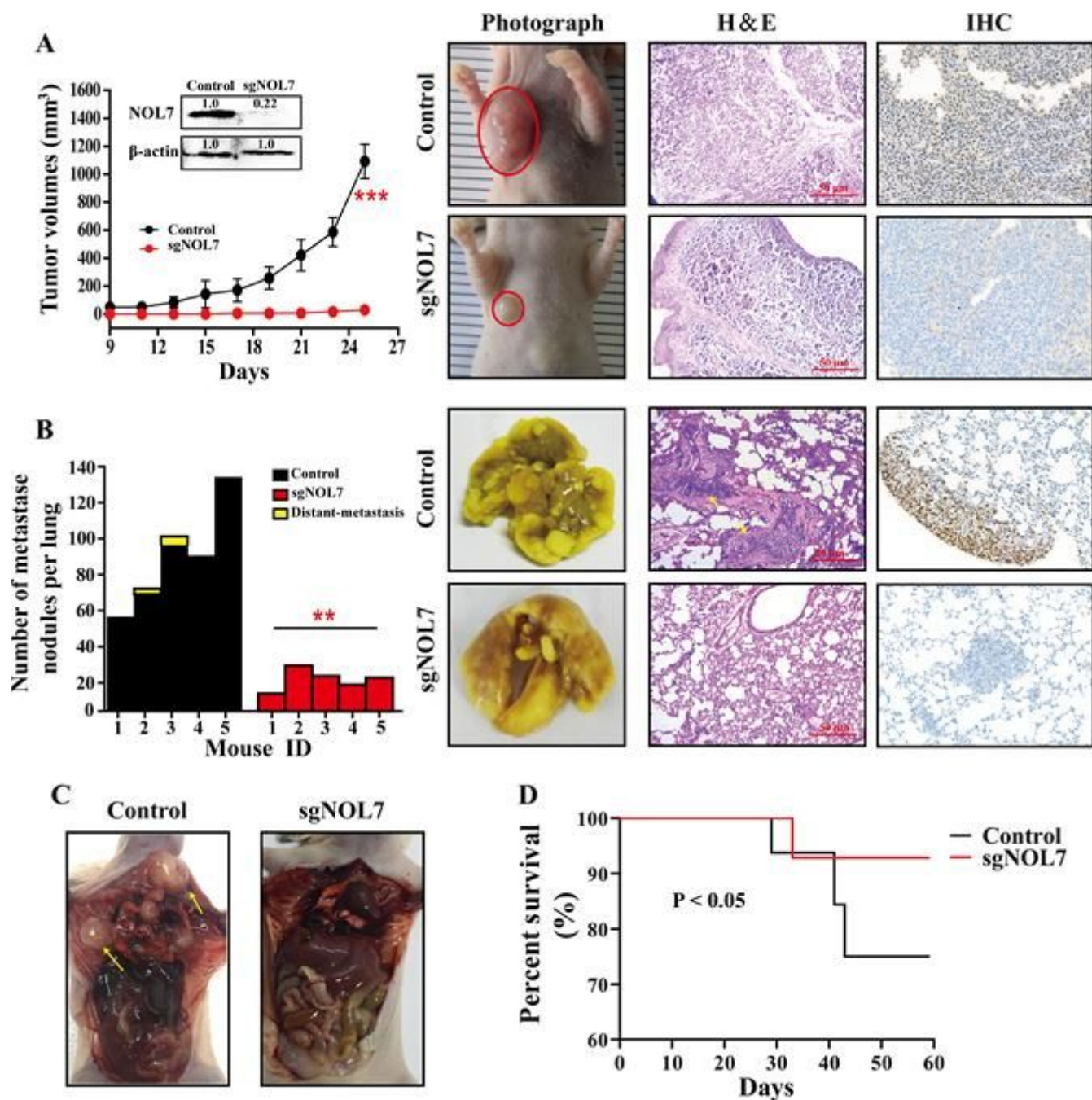


Figure 5

NOL7 is necessary for melanoma growth and metastasis in vivo. A. Reduced tumor growth in nude mice injected with NOL7-knockout cells, compared with control group. Inset shows the considerably depletion of NOL7 expression by CRISPR/Cas9 system. The mean tumor volume of 5 mice per group was shown in the left. Representative images of tumors and H&E staining are shown in right. IHC analysis indicates that NOL7 barely expressed in tumors which were formed by NOL7-knockout cells. B. NOL7 knockout decreased the number of lung metastatic nodules with nodules per mouse, as shown in the histogram (left). Likewise, representative photographs of H&E staining and IHC analysis are shown in right. C. Photographs show significant distant metastases in mice injected with control A375 cells, whereas no distant metastases in mice injected with NOL7-knockout A375 cells. D. Overall survival rate of mice

injected with control A375 cells and NOL7-knockout A375 cells in caudal veins. Low NOL7 expression is prognostic favourable in mice injected with A375 cells.

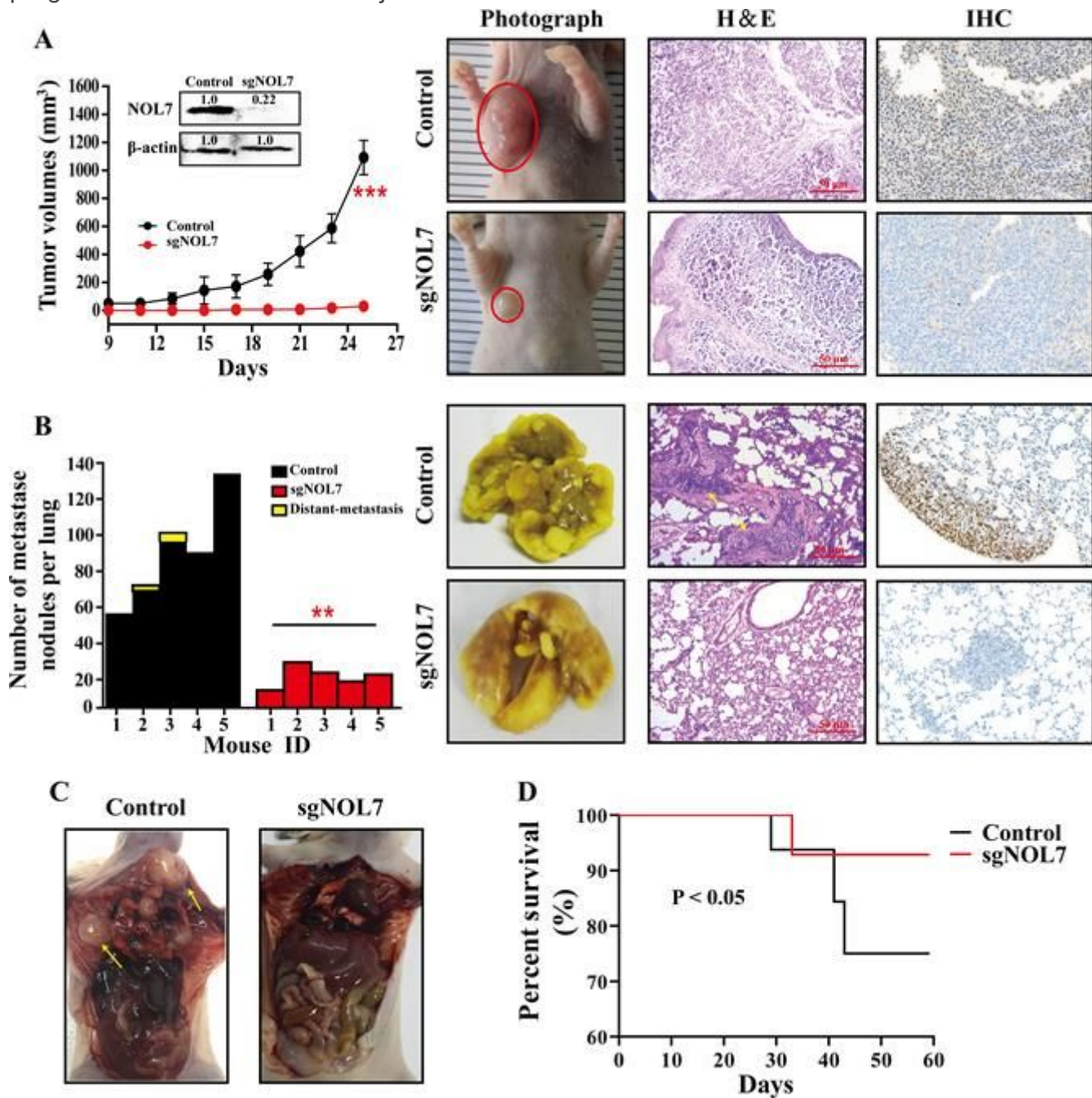


Figure 5

NOL7 is necessary for melanoma growth and metastasis in vivo. A. Reduced tumor growth in nude mice injected with NOL7-knockout cells, compared with control group. Inset shows the considerably depletion of NOL7 expression by CRISPR/Cas9 system. The mean tumor volume of 5 mice per group was shown in the left. Representative images of tumors and H&E staining are shown in right. IHC analysis indicates that NOL7 barely expressed in tumors which were formed by NOL7-knockout cells. B. NOL7 knockout decreased the number of lung metastatic nodules with nodules per mouse, as shown in the histogram (left). Likewise, representative photographs of H&E staining and IHC analysis are shown in right. C.

Photographs show significant distant metastases in mice injected with control A375 cells, whereas no distant metastases in mice injected with NOL7-knockout A375 cells. D. Overall survival rate of mice injected with control A375 cells and NOL7-knockout A375 cells in caudal veins. Low NOL7 expression is prognostic favourable in mice injected with A375 cells.

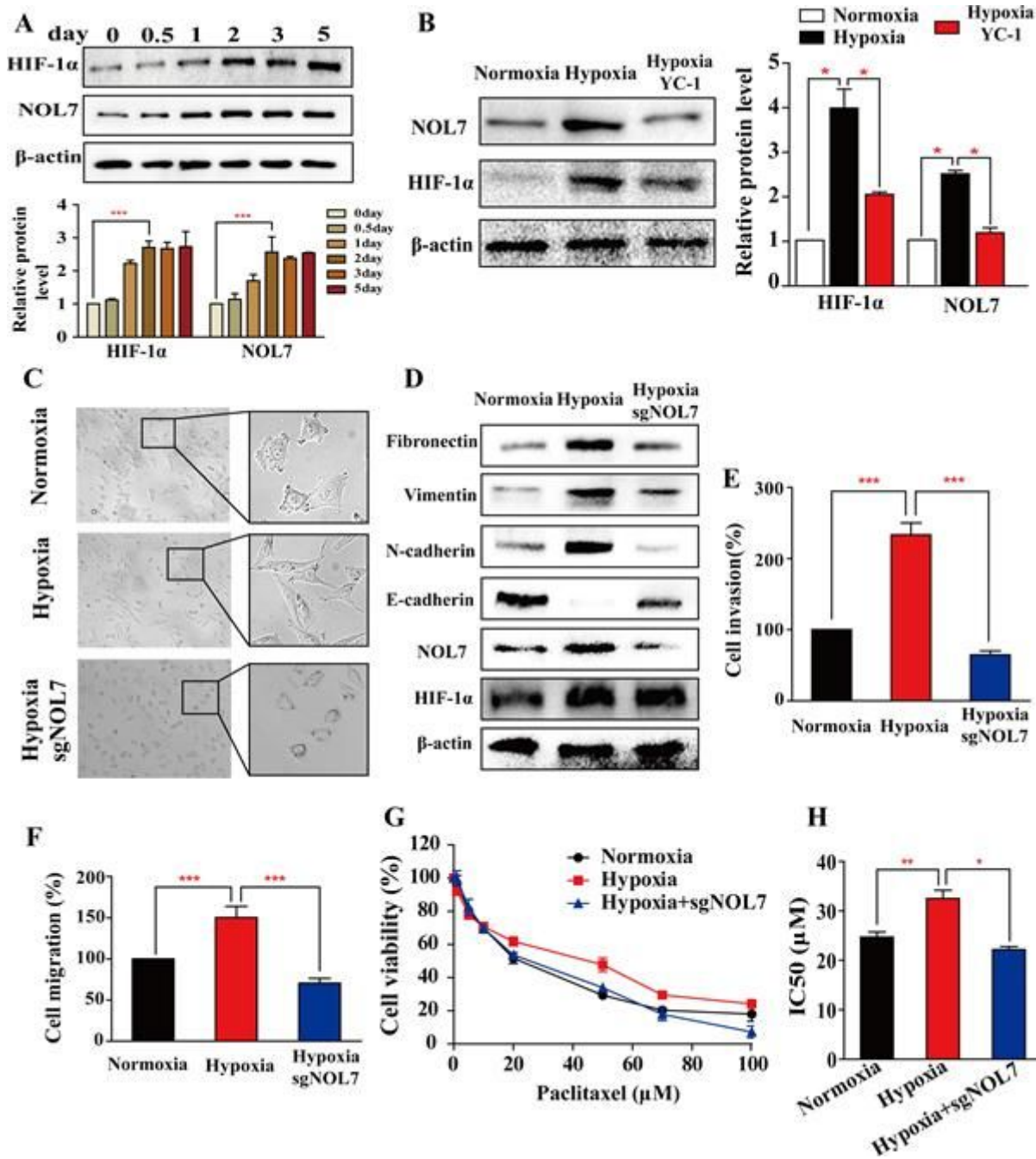


Figure 6

NOL7 participates in HIF-1 α -induced EMT, cell motility and chemotherapeutic resistance under hypoxia. A-B. Western blotting analyses showed concurrent NOL7 and HIF-1 α expression under hypoxia or treatment with YC-1 (HIF-1 α inhibitor). C-D. NOL7 depletion impaired the cell polarity and the expression of EMT markers induced by hypoxic condition. E-H. NOL7 depletion repressed hypoxia-induced cell migration, invasion and drug resistance to paclitaxel.

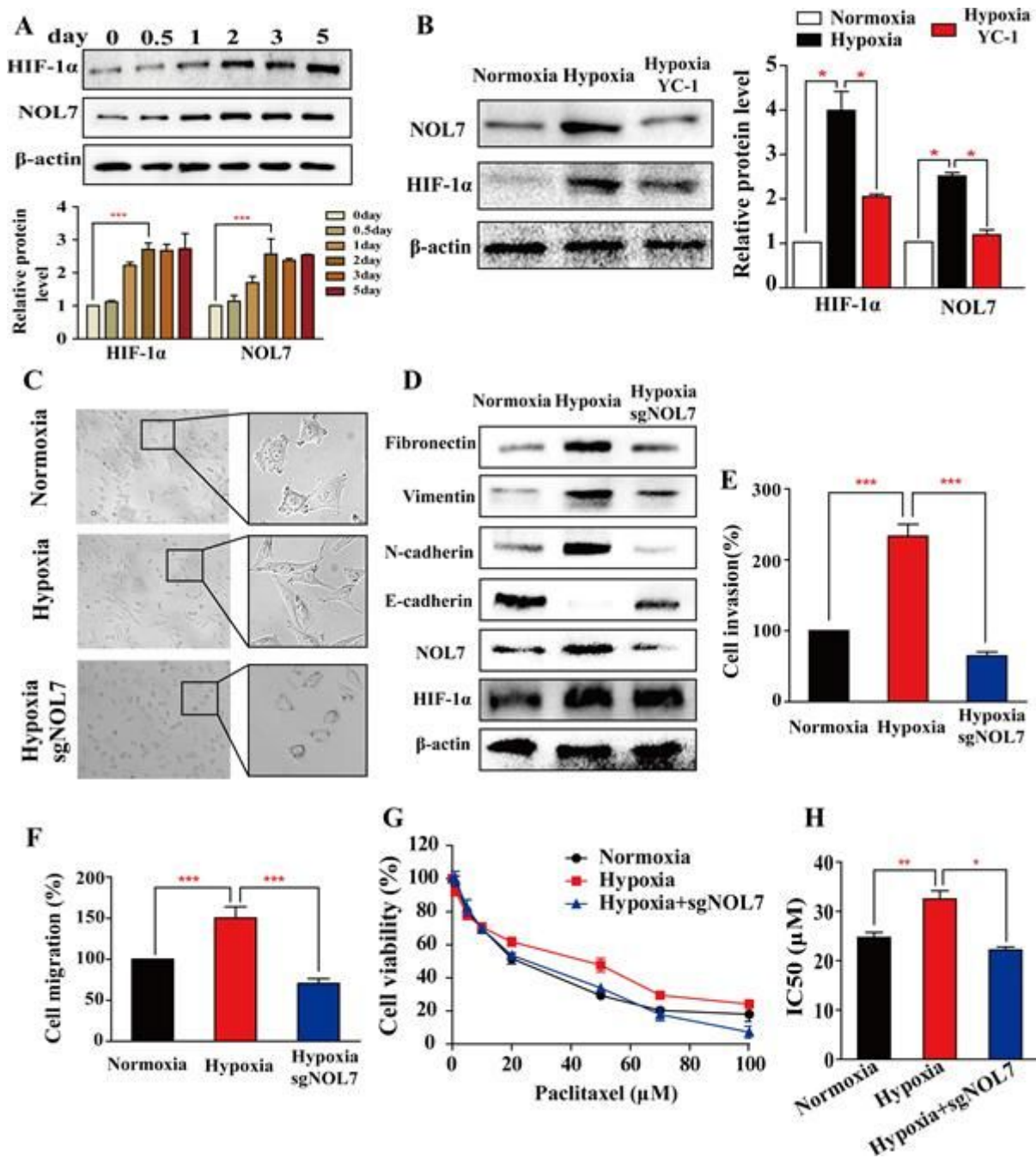


Figure 6

NOL7 participates in HIF-1 α -induced EMT, cell motility and chemotherapeutic resistance under hypoxia. A-B. Western blotting analyses showed concurrent NOL7 and HIF-1 α expression under hypoxia or treatment with YC-1 (HIF-1 α inhibitor). C-D. NOL7 depletion impaired the cell polarity and the expression of EMT markers induced by hypoxic condition. E-H. NOL7 depletion repressed hypoxia-induced cell migration, invasion and drug resistance to paclitaxel.

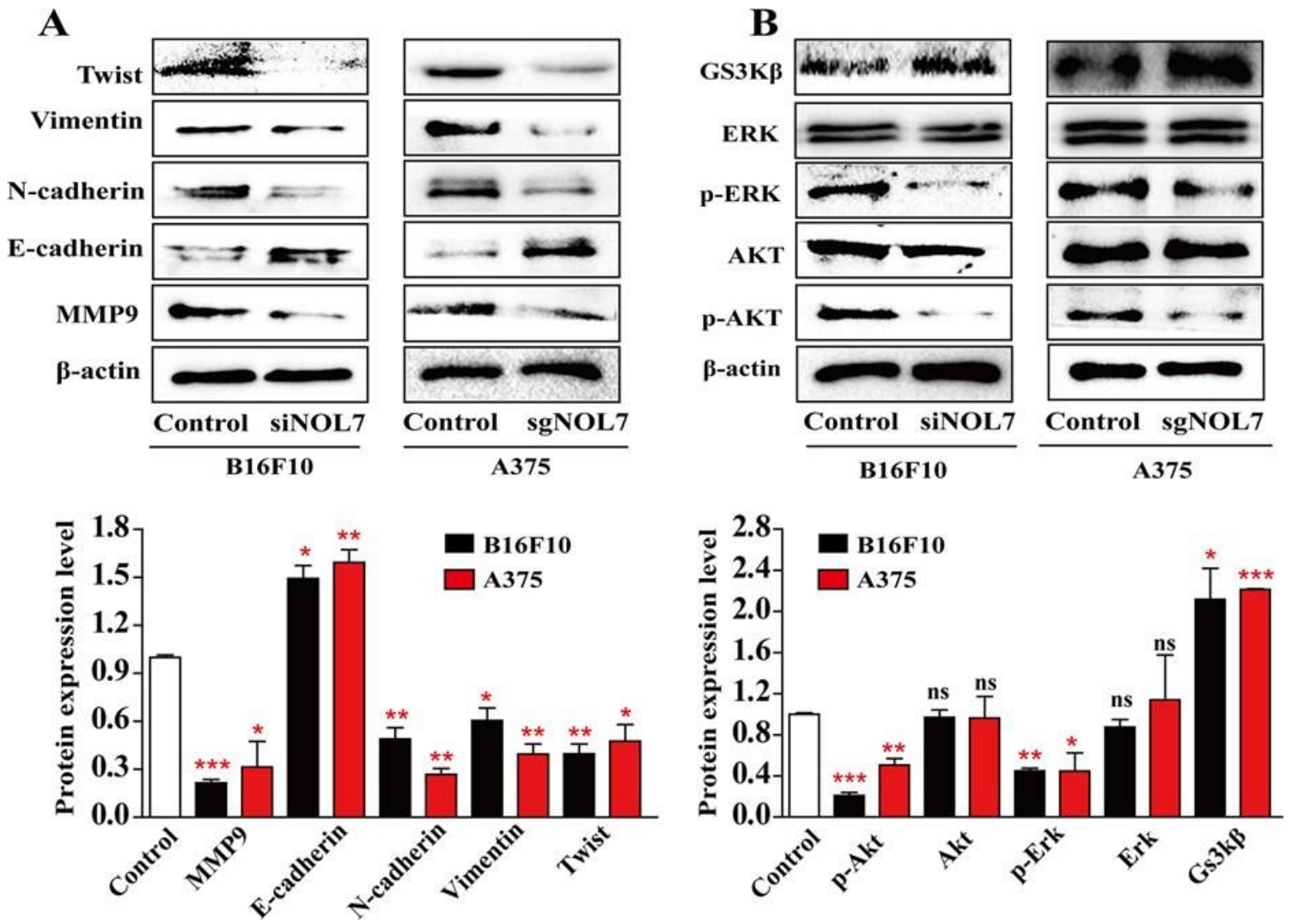


Figure 7

NOL7 induces EMT and activates the PI3K/AKT/ERK pathway in melanoma. A. NOL7 depletion increased the expression level of epithelial marker, E-cadherin and decreased the expression level of mesenchymal makers, N-cadherin, MMP9, Vimentin and Twist. B. Quantification analysis showed the inhibitory effect of NOL7 depletion on the PI3K/AKT/ERK signaling pathway through inhibiting the AKT and ERK phosphorylation and activating GSK3β.

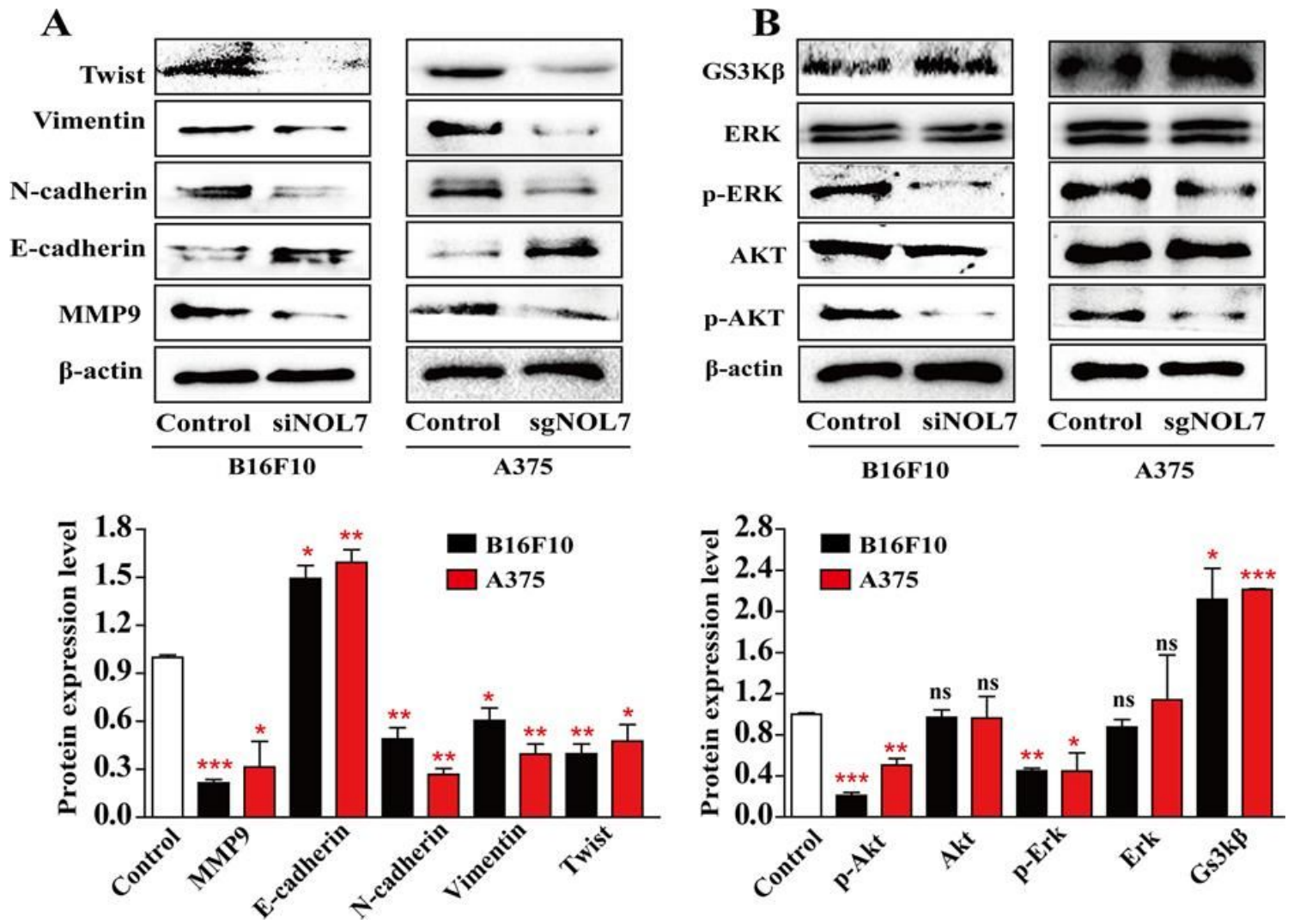


Figure 7

NOL7 induces EMT and activates the PI3K/AKT/ERK pathway in melanoma. A. NOL7 depletion increased the expression level of epithelial marker, E-cadherin and decreased the expression level of mesenchymal makers, N-cadherin, MMP9, Vimentin and Twist. B. Quantification analysis showed the inhibitory effect of NOL7 depletion on the PI3K/AKT/ERK signaling pathway through inhibiting the AKT and ERK phosphorylation and activating GSK3 β .

Supplementary Files

This is a list of supplementary files associated with this preprint. Click to download.

- [SupplementaryInformation.docx](#)
- [SupplementaryInformation.docx](#)